CROSS SECTIONS OF (p,pxn) REACTIONS IN Au^{197}

by

T. Murray Kavanagh

ABSTRACT

Cross sections of (p,pn), (p,p2n) and (p,p3n) reactions in Au^{197} have been measured by activation techniques for incident proton energies from the reaction thresholds to 86 Mev. Curves of cross section as a function of proton energy show similar shapes for the three reactions, and they rise from apparent thresholds at 16 Mev, 21 Mev and 30 Mev respectively, to peak cross sections of about 180, 145 and 150 millibarns for proton energies 30 Mev above their apparent thresholds. The cross sections then drop slowly for increasing proton energies. In the region of their peaks, the observed cross sections are an order of magnitude larger than the cross sections predicted by the statistical model. The reactions are interpreted in terms of initial quasi-free two-body interactions in the diffuse edge of the nucleus.

In connection with this work, the decay characteristics of the isomeric state in Au^{196} have been examined, and the experiments indicate that the isomer decays primarily by isomeric transitions, with a half-life of 9.5 ± 0.3 hours.

ACKNOWLEDGEMENTS

TABLE OF CONTENTS

LIST OF ILLUSTRATIONS

List of Illustrations

INTRODUCTION

This thesis describes measurements of cross sections for reactions of the type $(p,pxn)^{*}$ induced in gold by bombardment with protons of energies up to 86 Mev. These reactions, which may be described as inelastic proton scattering reactions, are of considerable interest since for a heavy target nucleus they cannot be interpreted in terms of the more familiarly accepted theories of nuclear reaction mechanisms. The work has been prompted in particular by two previous experiments.

Eisberg and Igo[1] have shown that the cross section for inelastic scattering of 31 Mev protons by heavy nuclei is an order of magnitude in excess of the predictions of the statistical model. The reaction mechanism involved is likely a direct surface interaction. A study of (p,pxn) reaction cross sections as a function of incident proton energy, for different values of x, and for a single heavy target nucleus, constitutes a study of this reaction mechanism.

---

*In this notation x is an integer, and in the present work takes the values 1, 2 and 3. The notation (p,pn) is usually taken to mean $(p,pn) + (p,d)$ since the techniques employed do not distinguish between different reactions leading to the same product nucleus. Similarly where $(p,p2n)$ is written, $(p,p2n) + (p,t) + (p,dn)$ is usually implied, and a similar ambiguity is contained in the notation $(p,p3n)$. In some instances a distinction will be made between the various possible reactions leading to the same product nucleus.

Secondly, Bell and Skarsgard[2] have shown that the sum of (p,xn) reaction cross sections for bismuth and lead nuclei exhibits a minimum for incident protons of about 25 Mev energy. It was thought that this drop in cross section may be due to competition from reactions of the type (p,pxn).

The cross sections that will be presented have been measured by activation techniques. Gold foils mounted with a graphite beam monitoring foil were bombarded in the internal beam of the McGill synchrocyclotron. K X-rays and gamma rays emitted by the product nuclei were identified and measured with a sodium iodide scintillation counter and a multi-channel pulse height analyzer.

In order to determine reaction cross sections from measurements of activity it is necessary to know the decay scheme of the nuclides involved. For this reason investigations have been carried out to clarify the decay characteristics of the isomeric state in Au^{196}.

A preliminary report on part of this work has been presented at the 1959 Congress of the Canadian Association of Physicists[3].

II

THEORETICAL BACKGROUND AND PREVIOUS EXPERIMENTAL WORK

Experimental work in the past several decades has offered a wealth of information on the structure of the atomic nucleus and on the way in which it reacts with energetic particles that are incident upon it. A rigorous analysis of the many-body problem that is involved is however impossible. In an attempt to interpret experimental results and to clarify our understanding of nuclear processes, recourse is taken to models which treat the physical situation in varying degrees of detail. Bohr's compound nucleus hypothesis, which in 1936 replaced the older single particle model, has had great success in the interpretation of experimental data. More recently it has been realized that the earlier single particle picture and Bohr's compound nucleus model have to be combined. This realization has had consequence in the various optical models. Further, it has been indicated that certain phenomena can be described in terms of a collective model, and that direct interactions occurring at the nuclear surface can be important. For a description of these models, the reader is referred to a review article by Moszkowski[4]. Several excellent review papers are also contained in a recent volume on nuclear reactions edited by Endt and Demeur[5].

According to the compound nucleus hypothesis, when an incident

particle enters a nucleus its energy is quickly shared among the nuclear constituents. After a time that is long compared to the time required for the incident particle to move a distance equal to the nuclear dimensions, this excited compound nucleus disintegrates, in a manner independent of the mode of formation. The emission of particles from the compound nucleus can be likened to an evaporation process and it is expected that the energy distribution of the evaporated particles will resemble a Maxwellian distribution, peaking at a few Mev energy. The angular distribution of the emitted particles is predicted to be symmetrical about 90 degrees to the incident particle direction. The total reaction cross section, if the incident particle energy corresponds to one of the energy levels of the compound nucleus, is given by

$$\sigma_R = \pi(R + \lambda)^2 B \qquad (II.1)$$

where R is the nuclear radius, λ the reduced de Broglie wavelength of the incident particle, and B a barrier penetration factor. For incident particle energies in excess of a few Mev, the energy levels of a complex nucleus will be closely spaced, and the reaction cross section becomes a smooth curve which approaches a value πR^2 at high energy. Theoretical total reaction cross sections for protons have been calculated by Blatt and Weisskopf[6] and Shapiro[7].

At bombarding energies in excess of about 50 Mev, and perhaps even lower, a different mechanism appears in the reaction processes[8].

The de Broglie wavelength of the incident particle becomes smaller than the nuclear dimensions, and the particle is capable of suffering localized interactions that can lead to the direct emission of highly energetic particles. The direct interaction, or "prompt internal nucleon cascade" process can be considered as taking place by primary quasi-free two-body collisions, which may result in the emission of a few prompt particles. Any residual energy appears as excitation of the residual nucleus. At higher energies the target nucleus appears partially transparent to the incident particle, and the total reaction cross section is reduced. The compound nucleus model extended in this way to include internal direct interactions is commonly called the statistical model.

Using the statistical model, Jackson[9] has calculated (p,xn) cross sections for heavy elements, for proton energies up to 100 Mev. Monte Carlo calculations based on known cross sections for two-body interactions were used to determine the contribution from internal nucleon cascades. These calculations also gave the distribution of residual energy after the emission of various numbers of prompt nucleons. The compound nucleus was assumed to decay only by neutron emission, since the high coulomb barrier strongly inhibits the evaporation of charged particles. Jackson considered the nucleus to be spherical, and of uniform nucleon density. The theoretical cross section for an individual (p,xn) reaction shows a steep rise above its own threshold, followed by a rapid drop above the threshold for the

emission of x + l neutrons. This rapid drop is a consequence of the
uniformly low kinetic energies of the nuclear constituents assumed
in the compound nucleus hypothesis. Peak cross sections are typically
of the order of several hundred millibarns. The narrow compound nucleus
peak is followed by a roughly constant cross section of about 150 milli-
barns extending to higher proton energies. This "tail" is due to prompt
internal cascades. The peak values of the successive (p,xn) cross sec-
tions increase as the coulomb barrier becomes less important, until
x = 4 (corresponding to about 40 Mev incident proton energy) and then
decrease owing to a decrease in the probability of compound nucleus
formation and to the fact that many processes are sharing the total
reaction cross section. The cross sections for reactions other than
(p,xn) reactions were found to be small, and the total reaction cross
section was taken to be the sum of the (p,xn) cross sections. This
calculated cross section curve, like the Shapiro curve, rises smoothly
from threshold to about 40 Mev, but then drops slowly due to nuclear
transparency effects.

Bell and Skarsgard[2] have published experimental (p,xn)
cross section curves for Bi^{209} and some isotopes of lead for proton
energies up to 90 Mev. The shapes of the individual (p,xn) curves
are in excellent agreement with the theoretical results of Jackson,
but the cross section sum curve shows a pronounced hump at about 20
Mev. This is in strong disagreement with the predictions of the
statistical model. It is well known that similar structure in total

reaction cross sections for neutrons can be successfully interpreted in terms of the optical model[10]. However, Jackson has pointed out that a complex potential consistent with proton elastic scattering results also predicts a total proton reaction cross section which is a monotonic function of energy.

Eisberg and Igo[1] have given evidence that a different mechanism can be involved in proton induced reactions. They investigated inelastic scattering of 31 Mev protons from lead, gold, tantalum and tin, and found total cross sections of about 290 millibarns, an order of magnitude in excess of the predictions of the statistical model, as exemplified by Jackson's calculations described above. Furthermore, the energy distribution of the scattered protons is approximately flat instead of being strongly peaked at low energy, and the angular distribution is strongly peaked forward. The results suggest that some sort of direct interaction is taking place, and the authors interpret the data in a rough qualitative way in terms of quasi-free two-body interactions in the diffuse nuclear edge. In such a diffuse edge protons with relatively long de Broglie wavelengths could be capable of suffering localized interactions. Eisberg and Igo show that their cross sections are approximately equal to the geometrical cross section of a diffuse edge of thickness r_o (where $r_o A^{1/3}$ is the nuclear radius). It is of interest to note that subsequent electron scattering experiments by Hofstadter[11] have shown that a diffuse edge of this dimension exists for the nuclear charge

distribution, and it has been indicated[12] that the neutron density distribution is similar.

Unexpectedly high cross sections for the inelastic scattering of 23 Mev protons by medium and heavy nuclei have been found by Cohen[13] and Cohen and Mosko[14]. They made careful measurements of energy distributions of scattered protons and the results indicate that the reactions proceed mainly by a direct rather than compound nucleus interaction. Cohen and co-workers also find evidence for direct (p,d), (p,t) and (p,α) reactions[14][15].

These low energy direct interactions have aroused considerable theoretical comment, and a number of interaction mechanisms have been proposed. Of these, three have been considered seriously. The first has already been mentioned, and involves quasi-free two-body interactions between the incident nucleon and a nucleon in the diffuse surface of the target nucleus. Quantitative calculations based on this mechanism[16] [17][18] are in good agreement with the experiments.

Secondly, a mechanism involving nucleon-nucleon collisions occurring throughout the nucleus has been considered by Hayakawa et al[19] and found to provide a successful fit to the experimental data. This result is in disagreement with the statistical model results of Jackson, but this in itself is not surprising since mean free paths of nucleons in nuclear matter as presently assumed in optical model calculations are longer than those assumed in the older compound nucleus model. On the other hand, Elton and Gomes[18] have raised

objections to this mechanism by showing that there is a high probability that nucleons resulting from collisions in the interior of the nucleus will be trapped into a compound nucleus by internal reflection in the optical potential.

The third mechanism that has been suggested involves the direct excitation of low-lying rotational states. Quantitative calculations for such a mechanism have been performed by Yoshida[20] and by Hayakawa and Yoshida[21], which show good agreement with the experimental data. From a comparison of (p,p'), (p,n) and (d,d') cross sections and energy distributions Cohen[22] concludes that collective excitations constitute the predominant reaction mechanism. However, Goodman[23] has pointed out that Cohen's "hypothesized dichotomy between inelastic scattering on the one hand, and pickup and stripping on the other" should be re-examined from the point of view of direct excitation of single particle shell model states.

A very interesting experiment by Griffiths and Eisberg[24] indicates strongly that direct proton inelastic scattering results from initial two-body collisions in the nuclear surface. These authors have measured angular correlations between protons with greater than 5 Mev energy emitted in (p,2p) reactions, for 40 Mev protons incident on nickel, copper and lead. A collision between an incident proton and a stationary free proton would result in a sharp angular correlation of the two outgoing protons at 90 degrees. If, on the other hand, the struck proton is bound, and has an initial

momentum, the angular correlation peak would be shifted from 90

degrees and broadened. The experimental results are best for

nickel, and the correlation curve has a broad peak at about 60

degrees. As pointed out by Griffiths and Eisberg, it is diffi-

cult to see how such a peak could arise if the direct interaction

mechanism involves excitation of low-lying rotational states. The

experimental results for nickel have been analyzed by McCarthy et

al [25] in an accompanying theoretical paper. From the position of

the peak of the angular correlation curve and the proton energy

spectra they estimate the average refraction of the emitted protons

in the nuclear potential, and conclude that the average distance

from the point of collision to the centre of the nucleus is about

7 or 8 x 10^{-13} cm (that is, collisions occur at the nuclear surface).

Furthermore, the width of the angular correlation curve determines

the momentum distribution of the struck nucleons. Analysis gives a

result $0.5 < p^2/2m < 1.5$ Mev, which is much lower than the momentum of

a nucleon in the nuclear interior. Finally, the ratio of the proba-

bility of emission of a pair of protons to the probability of emission

of a single proton indicates that the surface collision interaction

model is capable of explaining at least the majority of direct in-

elastic scattering events.

The cross section for proton inelastic scattering consists

of the following sum of individual reaction cross sections (where, of

course, the reaction notations are explicit since (p,d), (p,t), (p,tn)

etc. reactions are not included):

$$\sigma_{\text{inelastic}} = \sigma(p,p\gamma) + 2\sigma(p,2p) + \sigma(p,pn) + \sigma(p,p2n) + \text{---}$$
$$+ 2\sigma(p,2pn) + \text{-----} \qquad (\text{II.}2)$$

The experiments that have already been described involved direct
detection of the emitted protons, and so only the total cross sections
were obtained. Also, measurements were made only at isolated proton
energies. Cross sections for individual reactions in the sum given
above have been measured as a function of proton energy by several
investigators[26][27][28]. These measurements were mainly involved
with medium weight nuclei, and a notable feature of the results is the
high probability for proton emission resulting from (p,pn), (p,2p),
(p,p3n) and (p,p4n) reactions. These results can be interpreted in
terms of the surface collision model described above, but the reactions
are complicated for medium Z nuclei by a contribution from compound
nucleus interactions. Cohen et al[28] do however show (p,pn) cross
sections for tantalum and palladium for proton energies up to 23.5 Mev.
These reactions are likely due almost entirely to surface direct inter-
actions. The cross sections rise from thresholds at about 14 Mev to
about 100 millibarns and 200 millibarns respectively for 23.5 Mev
protons. Sosniak[29] has measured the (p,pn) reaction cross section
for gold, for protons of energies up to 32 Mev. The gold (p,pn) cross
section has also been measured by Yule and Turkevich[30] for proton
energies from 82 to 426 Mev.

The present experiments constitute the first comprehensive examination of (p,pxn) reaction cross sections for a heavy element over the energy range in which the surface direct interaction mechanism can be expected to predominate. Since cross sections are likely to be similar for the various heavy nuclei, an addition of (p,pxn) cross sections to the Bell and Skarsgard (p,xn) results should give an indication of the shape of the total reaction cross section.

III

METHOD AND APPARATUS

1. General Method

Gold target foils of 20 and 40 mg/cm^2 thickness were bombarded in the internal proton beam of the McGill synchrocyclotron. The sample foils were trimmed to the same size as a beam monitoring foil, and they were mounted on the radial probe so that they both received the same proton flux. The small attenuation of the proton beam in passing through the foils was neglected, but allowance was made for the degradation of proton energy. Bombardments lasted from five to twenty minutes with the full 1 microampere proton beam.

The product nuclides formed in the gold foils decay primarily by orbital electron capture. K X-rays and gamma rays which follow these capture events were detected with a calibrated NaI(Tl) scintillation counter. Pulse distributions from the counter were analyzed by a 28-channel pulse height analyzer in the early experiments, and later by a transistorized 256-channel instrument.

Beam monitoring was based on the reaction $C^{12}(p,pn)C^{11}$ taking place in graphite foils. The cross section for this reaction is well known. C^{11} decays with the emission of positrons, and the absolute yield of C^{11} activity was determined by detection of annihilation radiation following absorption of these positrons in

aluminum placed about the monitor sample. Counting was done with a second calibrated NaI(Tl) scintillation counter used in conjunction with a single-channel pulse analyzer and an automatic recording device.

In a sample of uniform thickness of n atoms/cm^2, the rate of production of active atoms through a particular reaction with cross section σ given by

$$\frac{dN}{dt} = \sigma pn - \lambda N \qquad (III.1)$$

where p is the beam current in protons per unit time, and λ is the radioactive decay constant for the nuclide in question. The disintegration rate at the end of a bombardment of duration t_B is

$$\lambda N = \sigma pn(1-\exp(-\lambda t_B)) \qquad (III.2)$$

and the observed initial counting rate is given by

$$R = c\lambda N \qquad (III.3)$$

where c is an efficiency factor depending on the counter efficiency (geometrical and intrinsic) and the number of radiations of the type counted, per disintegration.

We have for the reaction cross section

$$\sigma = \frac{R}{cpn(1-\exp(-\lambda t_B))} \qquad (III.4)$$

Combining equation (III.4) with a similar one for the

monitoring sample we have

$$\sigma = \frac{\sigma_m R c_m n_m (1-\exp(-\lambda_m t_B))}{R_m cn(1-\exp(-\lambda t_B))} \qquad \text{(III.5)}$$

where the subscripts m refer to the monitor sample. In cases where the bombardment time is small compared to the mean life of the nuclide being measured, (this holds for all gold nuclides, but not for the carbon monitor) equation (III.5) reduces to

$$\sigma = \frac{\sigma_m R c_m n_m (1-\exp(-\lambda_m t_B))}{R_m cn\lambda t_B} \qquad \text{(III.6)}$$

Target samples were bombarded at radii corresponding roughly to 5 Mev intervals in proton energy. Kirkaldy[31] has made a study of the energy distribution of the internal proton beam at various radii. The average of the distribution is estimated from the energy the protons would have at a given field and radius, if the orbit were always centered at the geometrical centre of the magnet, by subtracting an energy increment corresponding to a one inch reduction in radius. This is to correct for radial oscillations which cause the beam to circulate as though about a centre which itself rotates about the centre point of the magnet. The half-width of the energy distribution of the beam at any radius is given as the energy equivalent of

a 1.5 inch increment in the radius, and the shape of the distribution is asymmetrical and falls off more sharply at energies above the peak.

The effect of the energy spread on the shape of the measured (p,pxn) cross sections will be small, since the square of the half-width of any cross section curve is large compared to the square of the half-width of the proton energy distribution. The uncertainty in energy of the proton beam does, however, limit the usefulness of carbon as a monitor in the region of rapidly varying C^{12}(p,pn)C^{11} cross section.

2. Proton Beam Monitoring

Work by Bell and Skarsgard[32] has shown that direct monitoring of the proton beam by measurement of integrated proton current after it has passed through the foils is not feasible. It was found that there was an appreciable contribution to the current, probably from low energy ions drifting about in the vacuum, which was a function of radius, and which varied from time to time. Thus beam monitoring must be based on an activation measurement in which material with a known reaction cross section receives the same proton flux as the sample being studied. The reaction C^{12}(p,pn)C^{11} leading to a pure positron emitter with a half-life of 20.5 minutes is commonly used.

An improved monitoring foil has been developed for use in these experiments. Previous workers in this laboratory[2][29] used teflon foil ($(CF_2)_n$), which melts unless the beam current is strongly reduced. (For bombardments lasting more than a minute or so only about one tenth of the normal beam can be used). In the present work where cross sections are relatively low, a more heat resistant material was required. Teflon has a further disadvantage that the 20.5 minute carbon activity has to be separated from 112 minute F^{18} activity. This requires that decay curves be followed for about five hours.

Very satisfactory monitor foils were prepared by machining 1/4 inch diameter carbon spectrograph electrodes into thin sheets. For the earlier experiments this was done by mounting the carbon rods vertically on a milling machine, and making two parallel cuts just off the rod axis with a thin metal slitting saw. The saw was moved vertically in making these cuts. Foils 1/4 inch wide by 3/4 inch long and 0.010 inches thick were prepared in this manner, with a uniformity of thickness better than ± 0.0001 inches.

The activity induced in these foils was very high (in order to keep counting losses in the electronic circuits below 5 percent, source to counter distances of up to 1 metre were used), and the technique was later improved to enable thinner foils to be made. The carbon was cut roughly by the above method, and the "thick" foils were ground with a precision surface grinder. A

lucite block drilled with a pattern of fine holes which were con-
nected to a vacuum pump was attached to an iron plate, that was
in turn held to the magnetic grinder table. The rough carbon
sheets were placed over the small holes in the lucite block, and
were held by suction firmly enough for precision grinding. Foils
of about 0.0045 inches thickness, uniform to better than 0.0001
inches, were prepared for monitors in this manner. They were
remarkably strong and no extraordinary care was required in their
use.

The thickness of these foils (about 20 mg/cm^2) was
determined by weighing, and comparator measurement of surface area.
They were glued at the base ($\sim$ 3/4 inch from the tip where the beam
strikes) to an oversize piece of gold foil. After the glue dried,
the gold was trimmed with a razor blade to the same dimensions as
the carbon foil. The accuracy of the superposition was checked with
a microscope in several cases, and was found to be very satisfactory.

The carbon foils were transferred immediately after bom-
bardment to an automatic counting device. The carbon was placed
between two 1/4 inch thick discs of aluminum which absorbed all the
positrons, and the resulting annihilation radiation was counted with
a calibrated 1 1/2 inch high by 1 inch long NaI (Tl) scintillation
crystal (with a resolution width of 9.5 percent for the 0.511 Mev
photopeak), mounted on a Du Mont 6292 photomultiplier tube. The
anode pulses from the tube were fed through a cathode follower to

a Baird-Atomic linear amplifier and single-channel pulse height analyzer. The pulse analyzer window was set to pass only the total energy peak of the 0.511 Mev spectrum. The output pulses from the single-channel analyzer were passed through a scaler (which scaled the pulse rate down by factors of 64, 8 or 1) to a counting rate meter and Esterline-Angus chart recorder combination. A decay curve of the monitoring activity was automatically recorded on the Esterline-Angus chart. A fast Baird-Atomic scaler was used to count all pulses passing through the single channel, and this was used to check the linearity and absolute normalization of the chart recorder.

The sodium iodide crystal was calibrated to give the relative efficiency for total energy events as a function of source to counter distance, for distances from 10 to 100 cm. This calibration was accomplished using a decaying C^{11} source, with a portion of a decay curve being taken at each distance setting. The source was moved progressively closer to the counter at time intervals such that each point on the calibration curve was taken for the same counting rate. This procedure eliminated error due to counting losses and to any gain shift which might occur due to the high counting rates encountered at small distances with a long-lived calibration source strong enough to be conveniently counted at 1 metre.

The counter was calibrated absolutely by comparison of

total energy event counting rates for it and the calibrated counter

used in the gold measurements (see Section III.4). A F^{18} source was

used for this comparison. For purposes of calibration the total

energy peak from the monitor counter was defined as that portion

of the spectrum between the minimum above the Compton edge and a

point an equal distance beyond the maximum of the total energy peak.

At the time of this somewhat arbitrary definition a standard Na^{22}

source was counted, and this source, corrected for decay, was used

before each run to check the setting of the single-channel analyzer

and the general operation of the apparatus. It should be pointed

out that the above calibration does not include the factor 2 that

enters due to the two 0.511 Mev quanta emitted per positron annihi-

lation.

The $C^{12}(p,pn)C^{11}$ cross section that was used for moni-

toring is a composite one representing the results of several

investigations. A review of experimental information on this cross

section up to the end of 1955 is presented by Skarsgard[32].

Skarsgard used the composite curve published by Aamodt et al[33]

reduced by a factor 36/41 as recommended by Crandall et al[34], and

adjusted slightly to take account of the "smear" induced by the

energy distribution of the McGill proton beam. More recently

Whitehead and Foster[35] have made careful measurements of the

$C^{12}(p,pn)$ cross section for energies up to 40 Mev, and they

conclude that the 13 percent reduction of the Aamodt curves

suggested by Crandall et al should be made above about 32 Mev, but not below. In the present experiments beam monitoring was based on the conclusions of Whitehead and Foster. The composite cross section curve, adjusted slightly for energy smear, is shown in Figure 1.

It was pointed out earlier that uncertainties in the energy of the proton beam (which may amount to as much as 2 Mev) limit the usefulness of the carbon monitor below 25 Mev. The rapid variation in the carbon cross section in this region would lead to error in the determination of proton flux if the proton energy is not known accurately. This difficulty was avoided in the work of Bell and Skarsgard by the use of copper monitors at low energies. In the present work, however, only the two lowest points on the (p,pn) curve will be strongly influenced. They lie in a region of rapidly varying cross section, and errors in monitoring will not strongly affect the shape of the cross section curve. Furthermore, the results of Sosniak[29] give values of the Au^{197} (p,pn) cross section for 18 and 21 Mev protons monitored by the F^{19}(p,pn)F^{18} reaction, which does not vary so rapidly in this energy region. These data will define the shape of the (p,pn) cross section curve in the energy region where the present results are somewhat uncertain.

Fig. 1. $C^{12}(p,pn)C^{11}$ monitoring cross section. This curve is due to Aamodt et al[33], Crandall et al[34] and Whitehead and Foster[35], and has been adjusted slightly to take account of smearing due to the energy distribution of the McGill proton beam.

Figure 1

Figure 1

$C^{12}(p,pn)C^{11}$ Monitor Cross Section

CROSS SECTION (MILLIBARNS)

PROTON ENERGY (MEV)
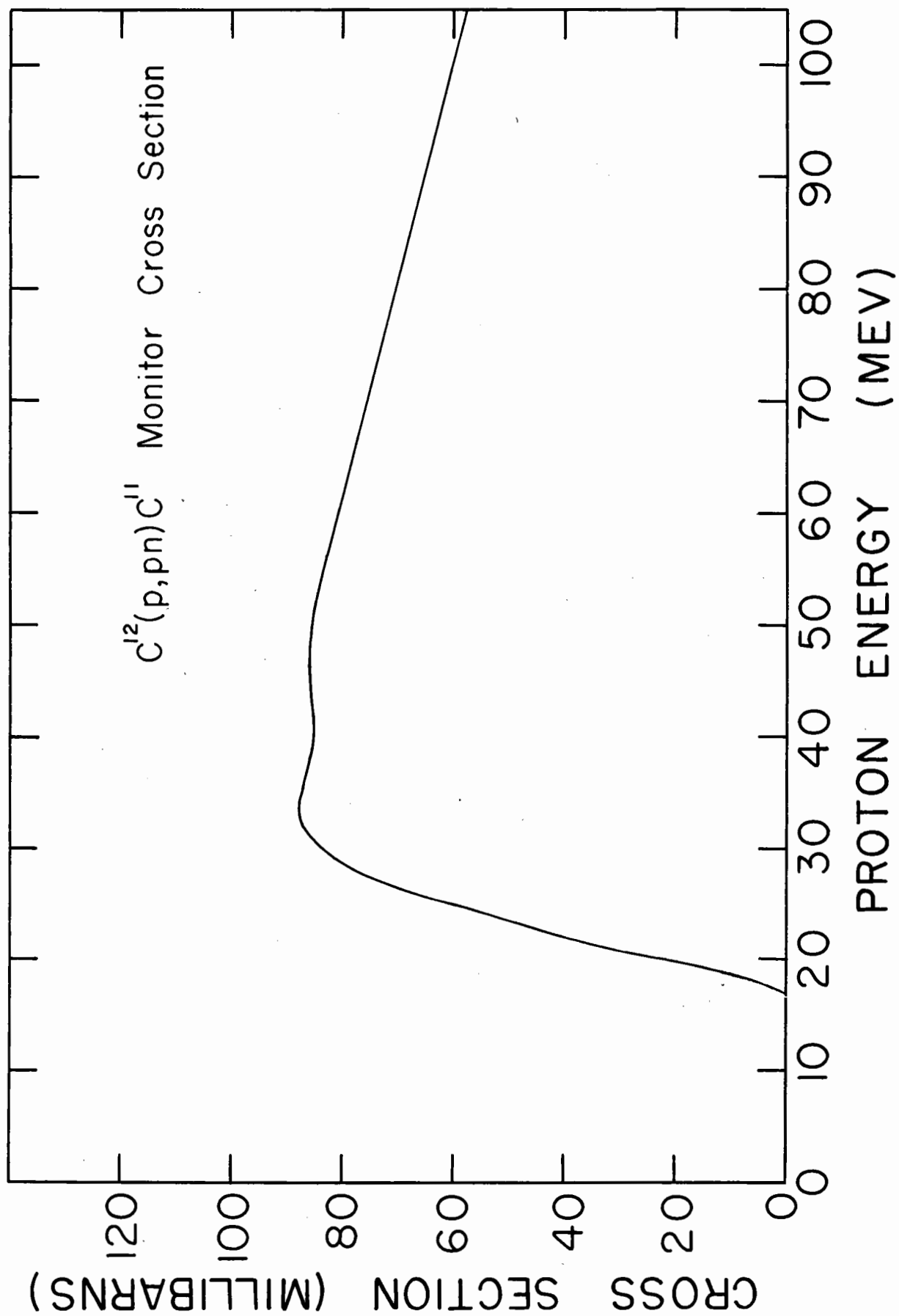
3. Removal of Mercury Contamination

Proton bombardment of gold leads to isotopes of gold through reactions of the type (p,pxn). In addition, large amounts of mercury will be formed by (p,xn) reactions, whose cross sections are several times larger than for (p,pxn) reactions. It is necessary to remove this mercury for two reasons:

(i) To prevent it from masking the activity of the gold isotopes which are produced in (p,pxn) reactions, and

(ii) To prevent the creation in the sample of the additional active gold atoms which result from decay of the neutron deficient mercury isotopes formed by (p,xn) reactions.

Mercury separation has been accomplished in these experiments by vacuum distillation techniques. Two different methods were used, and they will be called the "slow" and "fast" mercury removal techniques. In the case of the reaction $Au^{197}(p,pn)Au^{196}$ a slow mercury removal is satisfactory, at least up to about 62 Mev proton energy, since Hg^{196} is stable and hence cannot decay into Au^{196} (see Figure 2). A similar situation holds in the case of the (p,p3n) reaction leading to Au^{194}, since Hg^{194} has a half-life of about 130 days. A slow mercury removal technique, that is one in which mercury is removed following the bombardment, is however not satisfactory in the case of the (p,p2n) reaction, since the ground state

Fig. 2. Schematic representation of the
decay characteristics of nuclides resulting from
(p,pxn) and (p,xn) reactions in Au^{197}.
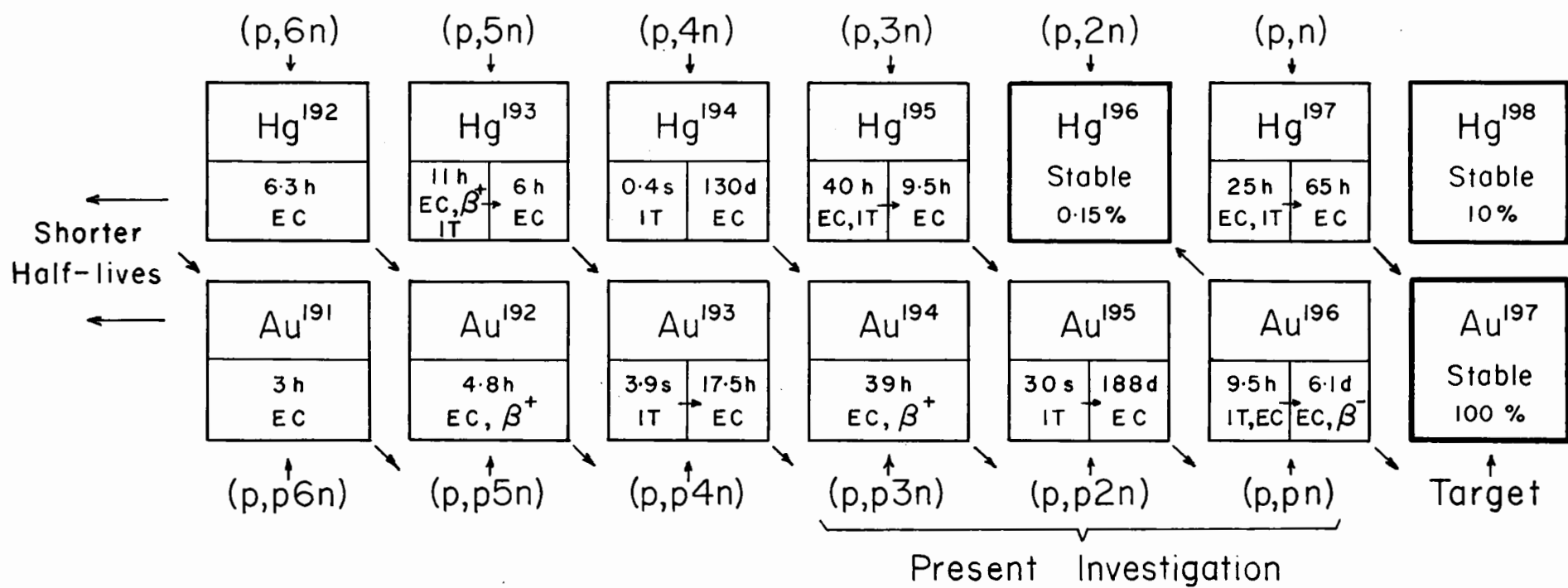
Figure 2

of Hg^{195} has a half-life of 9.5 hours. It is not possible to make corrections for mercury decay during a slow removal process since the (p,3n) cross section leading to Hg^{195} is not known, and more important, since an unknown amount of mercury is distilled into the cyclotron vacuum due to heating of the gold target by the proton beam.

A fast mercury removal technique was developed which involved electrical heating of the gold target during bombardment. Mercury was distilled into the cyclotron vacuum soon after its formation, and the gold samples were ready for counting immediately after removal from the cyclotron.

The fast removal of mercury, which was necessary for measurement of the (p,p2n) cross section also enabled extension of the (p,pn) and (p,p3n) studies above 62 Mev. At about 60 Mev, 57 minute Hg^{191} begins to be produced by a (p,7n) reaction, and with a slow removal technique a large amount of this decays into Au^{191} which subsequently decays into 3 day Pt^{191}. This nuclide interferes with measurement of the 6.1 day Au^{196} activity and the 39 hour Au^{194} activity. The fast removal technique significantly reduced this difficulty. (Small amounts of Pt^{191} from decay of Au^{191} formed by the (p,p6n) reaction, and probably from the decay of some Hg^{191} were detected, but no serious difficulty in analysis resulted).

(a) "Slow" Mercury Removal

After removal from the cyclotron, the target foils were heated to about 700 degrees centigrade in an evacuated fused silica tube, and the mercury that distilled off was trapped in a liquid air trap. Analysis of gamma ray spectra indicated that separation was complete in about 15 minutes, but in all cases heating was continued for an additional 45 minutes. As an additional check, one gold sample was "soaked" overnight in clean mercury after the initial separation, and a further distillation was then carried out. No reduction in activity was detected that couldn't be accounted for by decay of the gold isotopes.

The slow mercury removal method was used in the first ten bombardments. These bombardments yielded cross sections for the (p,pn) and (p,p3n) reactions from threshold to 62 Mev.

(b) "Fast" Mercury Removal

The rapid mercury removal technique involved direct heating of the gold target during bombardment by passing an electric current through it. The gold targets were 20 mg/cm^2 thick (half the thickness used in the earlier experiments) by 3/4 inch long and 1/4 inch wide, with a 0.010 inch wide slit cut longitudinally along the centre of the target from the base to within 1/8 inch of the target tip. This longitudinal slit provided electrical

terminals which were both at the base of the target, and increased the effective electrical resistance of the foil. This form of target had the added advantage that the proton beam could be conveniently monitored with graphite, since the target tip could be cut to the shape of a monitor foil.

Targets were made by clamping an oversize piece of gold foil in a lucite jig which exposed a portion of the gold in a rectangular slot the same size as the monitor foils. A template was inserted in this slot to guide a razor blade in cutting an approximately 0.010 inch wide strip from the gold longitudinally along the centre of the slot, to within 1/8 inch of the end of the slot. The carbon monitoring foil was then placed in the slot and cemented to the gold at its base, with a 10 mg/cm^2 thick mica sheet, slightly smaller in the other dimensions than the carbon foil insulating it electrically from the gold. When the glue was dry, the carbon-mica-gold sandwich was removed from the jig, and the gold foil was carefully trimmed with a razor blade to fit the carbon monitor. This method provided gold targets of the desired form which were accurately matched to the monitoring foil. It should be pointed out that the slit down the centre of the target will slightly alter the average gold thickness in $atoms/cm^2$ relative to that of the monitor. However, since about 80 percent of the incident protons strike in the first 1/8 inch back from the target tip[31], the effect of the slit on the monitoring procedure is negligible.

The target assembly was mounted in a special target holder which provided electrical connections between the base of the gold foil and the current leads in the cyclotron probe. Currents of about 5 amperes were sufficient to heat the target tip to bright red heat (about 800 degrees). Due to thermal conduction in the gold the red heat was confined to the first 1/4 inch back from the target tip, but in any case there is negligible proton flux beyond this portion of the target.

In order to prevent destruction of the fragile gold targets due to the forces involved when 5 amperes of current flow through it in the 16000 gauss magnetic field of the cyclotron, 100 kilocycle alternating current was used for heating. (Early experiments using power from an audio generator-power amplifier arrangement indicated that frequencies in excess of 10 kilocycles were required). The 100 kilocycle power was provided from a signal generator located in the cyclotron control room, feeding a tuned power amplifier located near the cyclotron probe. A special air-cored output transformer with a step-down ratio of 180 turns to 1 turn was constructed to match the output tubes of the amplifier to the 1/4 ohm DC resistance in the leads and the gold target. (The resistance of the gold itself was only about 0.02 ohms). It was also necessary to series tune out the inductance of the leads from the amplifier to the gold foil.

In order to maintain the temperature of the gold foil between about 800 degrees and its melting point (1060 degrees) it was necessary to control the temperature remotely during the bombardment and in particular to compensate for additional heating due to the proton beam. The temperature monitoring of the hot gold was done by measuring its resistance. A 100 kilocycle signal proportional to the heating current was obtained from a pickup coil on one of the current leads, and a voltage signal was taken from directly across the gold foil. These signals were fed through coaxial cables to the cyclotron control room. The current signal was adjusted to be in phase with the voltage signal by means of a simple low pass RC network (which also suppressed harmonics created in the pickup coil) and the signals were applied to the X and Y deflection plates of a Du Mont 304H cathode ray oscilloscope. The resulting straight line Lissajous figure had a slope proportional to the resistance of the gold foil. DC restoration was used on both signals so that the line rotated about its lower extremity with changes in resistance. A change in temperature of the gold foil from about 800 to 1000 degrees was indicated by a 1/4 inch deflection of the upper end of the scope trace, when the line was initially inclined at 45 degrees.

Before each bombardment the temperature of the mounted target foil was adjusted in the cyclotron to about 800 degrees by means of a helipot on the input of the power amplifier. The

temperature of the foil was estimated from visual observation
through a window in the side of the cyclotron vacuum chamber.
(The observer's eye was "calibrated" with an optical pyrometer,
and temperature estimates were probably accurate to within 75
degrees). The gains of the X and Y amplifiers in the oscil-
loscope used for temperature monitoring were then adjusted so
that the scope trace was inclined at 45 degrees. (The oscil-
loscope graticule was rotated 45 degrees to give a system of
reference). The slope of the line was maintained slightly on
the "hot" side of 45 degrees throughout the bombardment by ad-
justing the output of the signal generator. Heating was con-
tinued for 10 minutes after the end of the bombardment.

An experiment was performed to test the speed of mercury
removal in the above technique. A gold target of the same form as
used in the cross section experiments was bombarded at reduced
beam at an energy such that large amounts of mercury would be
produced. The low beam current was used to prevent mercury boil-
off due to heating by the beam. This sample was mounted in an
evacuated glass apparatus constructed to allow electrical heating
of the gold. A liquid air trap was provided to trap mercury that
distilled off. K X-rays from the mercury and gold isotopes present
were observed with the single-channel scintillation spectrometer
and recording device used for measurement of carbon monitoring
activities (Section III.2). A conical lead collimator over the

counter discriminated against radiation which might originate from mercury on the walls of the glass apparatus. The Esterline-Angus recorder record of the counting rate, before and after the heating current was turned on, is reproduced in Figure 3. The counting rate dropped rapidly when heating began, indicating a "mean life" for a mercury atom in the foil before boil-off of about 40 seconds.

The requirement which must be met in such a rapid mercury separation is that this mean life before boil-off be small compared to the mean life for radioactive decay. The results quoted above satisfy this requirement in the case of Hg^{195}. However, some very small amounts of mercury were present following bombardment in targets bombarded in the energy region of high (p,3n) cross section, and all such targets were subjected to further heating by the "slow" removal technique.

Further experiments were performed to check the effectiveness of the mercury removal. In several cases targets were bombarded at an appreciably lower temperature, and no significant change in the measured (p,p2n) cross section resulted. A more important check was offered by a sample bombarded at 23.2 Mev. This energy is probably below the (p,p2n) threshold, yet well above the (p,3n) threshold (where here the (p,p2n) reaction is distinguished from the (p,t) reaction, which leads to the same product nucleus, but which is energetically favoured by about 8.5 Mev). Cohen and Rubin[15] have shown that the $Au^{197}(p,t)Au^{195}$ cross section

Fig. 3. Results of a radioactive tracer ex-
periment performed to measure the rate of vacuum
distillation of mercury out of 0.0005 inch thick
gold foil heated electrically to about 800 degrees
centigrade.

Figure 3   32a
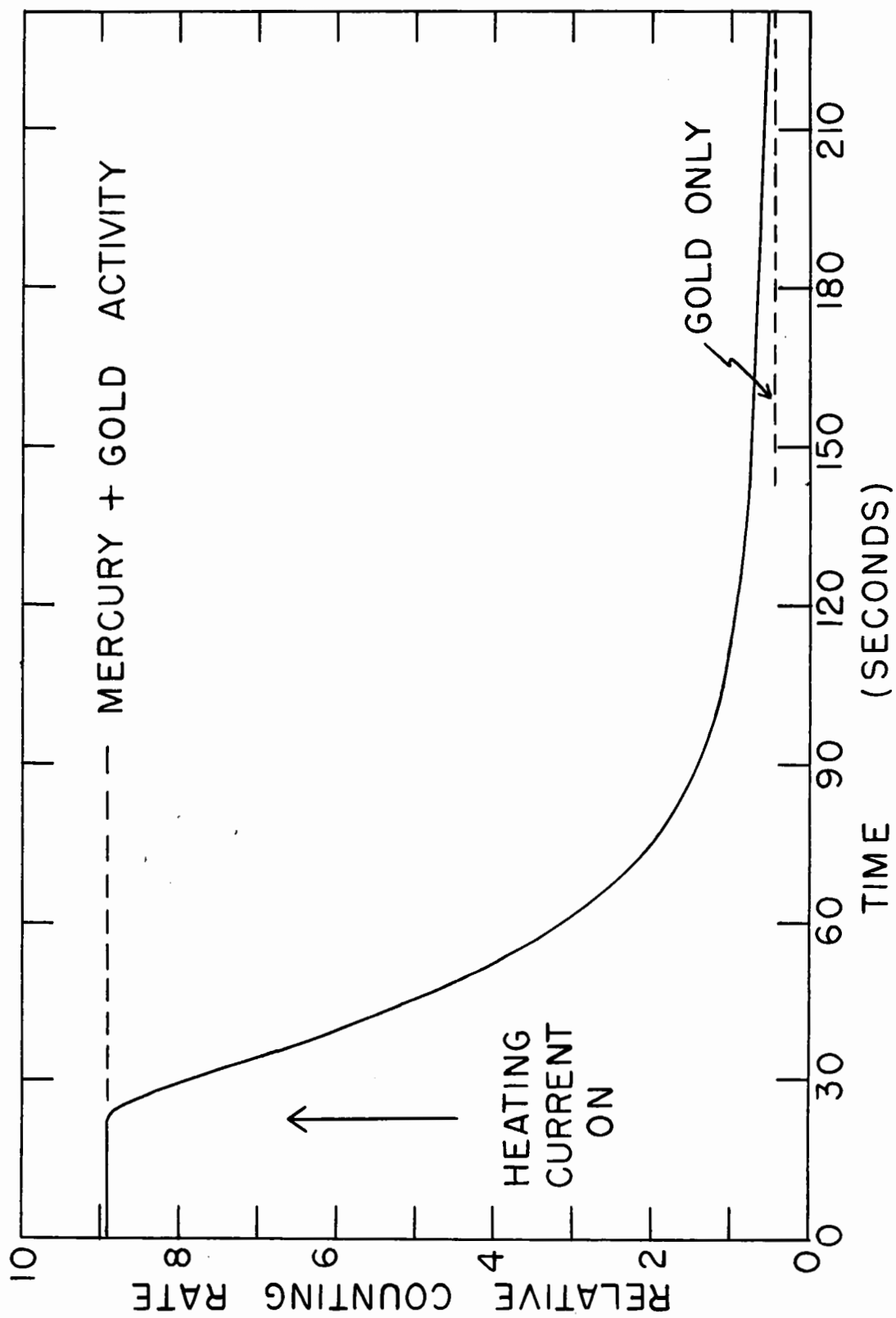
is 9.5 millibarns for 23 Mev protons. Since the (p,3n) cross section leading to Hg^{195} is about 500 millibarns at this energy, the decay of only 1 percent of this mercury before its removal would result, in the present experiments, in an apparent (p,p2n) + (p,t) cross section at least 50 percent greater than Cohen's (p,t) value. Instead, the measured cross section is 15 percent lower than Cohen's value, and it was concluded that more than 99 percent of the mercury formed in (p,3n) reactions was removed from the samples before it decayed into Au^{195}.

4. Gamma Ray Spectroscopy

K X-rays and gamma rays that follow electron capture events in the radioactive nuclei formed in (p,pxn) reactions were identified and counted with a scintillation spectrometer. For most measurements the detector consisted of a 1 1/2 inch diameter by 1 inch high NaI(Tl) crystal (with a resolution width of 8 percent for the Cs^{137} 662 kev photopeak), mounted on an RCA 6342A photomultiplier tube. After passing through a cathode follower, the pulses from the counter were analyzed by a multichannel kicksorter.

In the early experiments pulse-height analysis was done with a 28-channel kicksorter designed and built in this laboratory. This instrument is described elsewhere[36]. Later a transistorized 256-channel Technical Measurements Corporation instrument was used.

This kicksorter can be used in 4 sections of 64 channels (or
2 sections of 128 channels), and spectra in the present work
were analyzed into 64 channels. This facility was of great
convenience when many samples were being counted. Spectra were
recorded for two different amplifier gain settings to conveniently
measure K X-rays and higher energy gamma rays. The two spectra
were recorded independently in the first 2 sections of 64. Room
background for the two gain settings was measured once before each
series of counts and stored negatively in the third and fourth
sections of 64. These inverted spectra could then be transferred
to the empty first and second quarters before each count, effecting
automatic background subtraction. Also, the kicksorter can be set
to record "live" counting time, thus correcting automatically for
counting losses. Both digital and analogue readouts are provided.

The scintillation counter used in these measurements had
been calibrated previously[32]. The calibration curves give the
probability of an emitted photon being registered as a total energy
event, as a function of photon energy, and of source to counter
distance. A measurement of the counting rate of total energy
events for a given component in the gamma ray spectrum thus yields
the emission rate of that radiation from the source.

In order to determine the counting rate for total energy
events for a given gamma ray component, the Compton continuum from
higher energy gamma rays is subtracted from below the total energy

peak. A general method for subtracting Compton background has

been described by Skarsgard[32]. In the present work, however,

the peaks were cleanly defined, and no analytical procedure was

required. It should be noted that for K X-rays the total energy

peak is taken to include the small lower energy peak due to the

escape of iodine X-rays from the crystal (see Figure 4).

Curves of counting rate as a function of time were plotted.

The half-lives from these decay curves, together with the energy of

the radiation being counted, served to identify the reaction products.

Sources were counted with low geometrical efficiency with

the spectrometer in order to prevent summing effects. Any two

photons registered by the scintillation counter within about 0.5

microseconds of each other will give rise to a single pulse from the

photomultiplier, whose height is equal to the sum of the pulse

heights that would result from each photon separately. In order to

prevent summing of photons emitted in coincidence, source to counter

distances were never less than 5 cm.

The gamma ray spectrometer described above was used for

measurement of activities due to (p,pn) and (p,p3n) reactions. Low

efficiency was essential in these measurements, since peaks in the

spectra due to summing effects would make it extremely difficult

to separate the two activities from one another, and from activities

due to other reactions ((p,p4n), (p,p5n) etc). However, the Au^{195}

activity resulting from the (p,p2n) reaction has a half-life of 188

Fig. 4. Pulse height spectrum from platinum
K X-rays which follow K-capture in gold, detected
by a sodium iodide scintillation counter (crystal
size 1 1/2 inches by 1 inch). The smaller peak is
due to the escape of iodine K X-rays from the cry-
stal.

Figure 4 36a
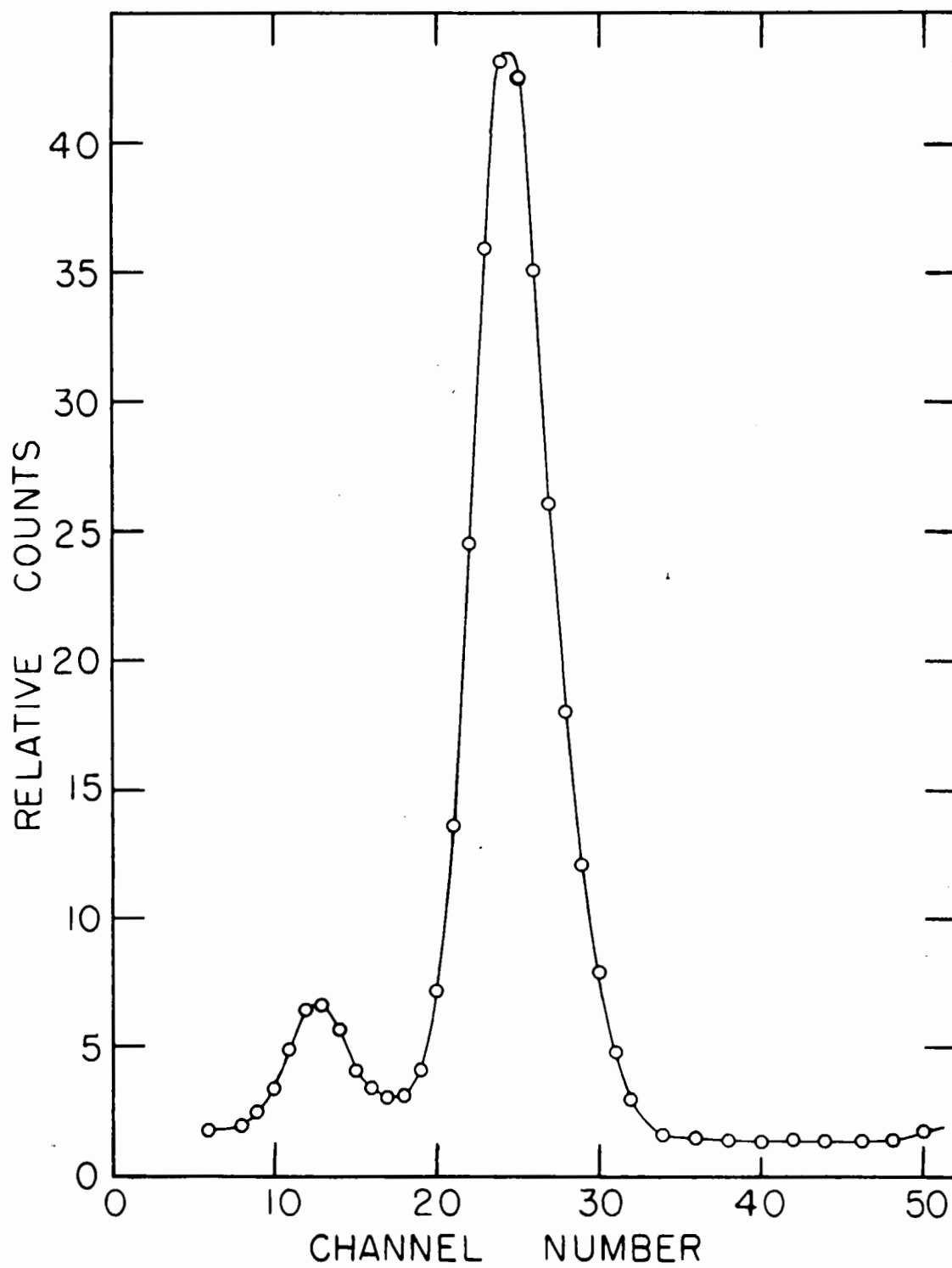
days, and after about two months can be counted free of interfering activities. Since these sources were very weak it was advantageous to count them with a counter of high geometrical efficiency. No attempt was made to separate the various components in the gamma ray spectrum, and cross sections were based on total counting rates, including "sums". It will be shown later that this integration of the whole spectrum, with high efficiency counting, makes results much less sensitive to uncertainties in the decay scheme.

A scintillation counter with about 90 percent efficiency was used for Au^{195} measurements. The two sodium iodide scintillation counters previously described (in this section, and section III.2) were arranged to face each other, in contact, with the gold samples held tightly between the flat surfaces of the two crystal cans. The output cables from the two cathode followers were both connected to the kicksorter input terminal. The gains of the two counters were made equal by adjusting the high voltage to the photomultipliers. This counting arrangement functioned like a single sodium iodide crystal with about 95 percent geometrical efficiency.

5. Determination of Absolute Disintegration Rates

(a) Factors Entering Into Disintegration Rate Determinations

In order to determine absolute disintegration rates for

a particular nuclide from measured counting rates of components in the gamma ray spectrum, it is necessary to know the following:

i. Branching Ratios

When measurements are based on a gamma ray which accompanies the decay of a particular level in the daughter nucleus it is necessary to know the proportion of electron capture events which lead to population of this level. If any disintegration takes place by β+ or β- emission the branching ratios for these decays must be known.

Branching ratios are of lesser importance when disintegration rates are to be based on K X-ray yields, unless the transition energies are low.

ii. Ratio of K to Total Electron Capture

If disintegration rates are to be based on measurements of K X-rays, the proportion of the total electron capture events proceeding via the K-shell must be known. In some cases experimental values for these ratios are available. Theoretical ratios can be found from the computations of Brysk and Rose[37] if the disintegration energy of the electron capture process and its order of forbiddenness are known. Disintegration energies can be measured if a small positron branch occurs in the decay, and in some instances estimates can be made from mass differences.

Fortunately, the variation of the K to total capture ratio with disintegration energy is slow except near the energetic threshold for electron capture.

Brysk and Rose give theoretical transition probabilities for electron capture in the various shells. Wave functions for the bound-state electrons were corrected for the finite size of the nucleus, and the effect of screening. The greatest contribution to the total capture apart from K captures comes from the L_I-subshell. The L_I/K capture ratio is independent of the transition energy and the order of forbiddenness for $W_O \gg W_L - W_K$ (where W_O is the energy difference between the disintegrating nucleus and the level in the daughter nucleus to which the decay proceeds, and W_K and W_L are the energies of the K and L electrons, including the electron rest mass). For transition energies near the threshold for K-capture the L_I capture probability is a strong function of energy. Brysk and Rose plot the L_I/K capture ratio as a function of W_O for allowed transitions, and the corresponding values for ordinary first forbidden transitions, which are of interest in the present work, are obtained by multiplying by $(W_O + W_{L_I})^2/(W_O + W_K)^2$. The L_{II}/L_I ratio is plotted as a function of Z and does not depend strongly on the transition energy or the order of forbiddenness. The L_{III}/L_I capture ratio is always negligible for allowed and ordinary first forbidden transitions. For higher shells the capture probability falls off roughly inversely

as the third power of the principal quantum number.

iii. K Fluorescence Yield

The creation of a K-shell vacancy in an electron capture event is not always followed by the emission of a K X-ray. The K fluorescence yield is defined as

$$\omega_K = \frac{X_K}{V_K} = \frac{X_K}{A_K + X_K} \tag{III.7}$$

where: X_K is the number of K-shell vacancies resulting in K X-rays,

A_K is the number of K-shell vacancies resulting in Auger electrons, and

V_K is the number of primary K vacancies.

A compilation by Bergstrom[38] gives $\omega_K = 0.95$ for gold, with a probable error of the order of 1 percent.

iv. Internal Conversion Coefficients

Internal conversion of gamma rays which follow electron capture can give rise to additional K X-rays if the conversion takes place in the K-shell. A correction must be made for these additional X-rays if total disintegration rates are to be based on measurements of K X-rays. A correction for internal conversion in all shells must be made if disintegration rates are to be based

on the measured counting rate for a particular gamma ray.

In the present work experimentally determined conversion coefficients, or theoretical values[39] based on known gamma ray multipolarities were used for the above corrections. In all cases experimental electron capture branching ratios were available. Skarsgard[32] has described a summing technique for determining the correction necessary to measured K X-ray counting rates if detailed information on the decay scheme is not available.

v. Self-Absorption in the Active Sample

The self-absorption in the gold samples was calculated from published absorption coefficients[40] by assuming an effective absorber thickness of half the thickness of the sample. The attenuation of 68.4 kev X-rays in a gold sample 45 mg/cm^2 thick amounts to 5 percent.

(b) Absolute Disintegration Rate Calculations: General Case

In the discussion which follows, reference will be made to the example decay scheme shown in Figure 5.
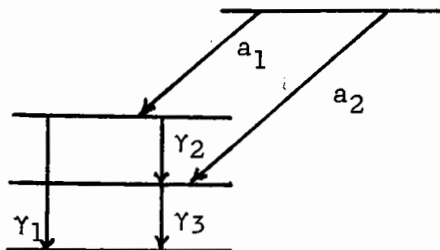
Figure 5: Example decay scheme

a_1, a_2 are the branching ratios for the two electron capture branches,

f_1, f_2 are the K to total capture ratios for the two branches,

α_{jK}, α_{jT} are the K and total conversion coefficients for the gamma transition γ_j,

n is the fraction of decays from the upper level in the daughter nucleus resulting in emissions of γ_1, and

ω_K is the K fluorescence yield.

Let us first suppose that the disintegration rate is to be determined from R_K, the measured counting rate for K X-rays. If the efficiency of the counter for detecting K X-rays is ε_K, (this includes geometrical and intrinsic efficiencies) then the rate of emission of K X-rays from the sample is R_K/ε_K, and the absolute disintegration rate is given by

$$\lambda N = \frac{R_K}{S_K \varepsilon_K \omega_K} \left\{ \left[a_1 f_1 + a_2 f_2 \right] + \left[\frac{a_1 n \alpha_{1K}}{1+\alpha_{1T}} + \frac{a_1 (1-n) \alpha_{2K}}{1+\alpha_{2T}} + \frac{a_1 (1-n) \alpha_{3K}}{1+\alpha_{3T}} + \frac{a_2 \alpha_{3K}}{1+\alpha_{3T}} \right] \right\}^{-1} \quad \text{(III.8)}$$

The first square bracketed term describes the formation of K-shell vacancies by electron capture, and the second term the contribution from internal conversion of gamma rays. S_K is an attenuation factor due to self-absorption in the sample.

If disintegration rates are to be based on the measured counting rates of say γ_3, then we have

$$\lambda N = \frac{R\gamma_3}{S\gamma_3 \varepsilon \gamma_3} \left[\frac{a_1(1-n)}{1+\alpha_{3T}} + \frac{a_2}{1+\alpha_{3T}} \right]^{-1} \qquad \text{(III.9)}$$

where $R\gamma_3/\varepsilon\gamma_3$ is the total emission rate of gamma rays of the

type γ_3. $S\gamma_3$ corrects for self-absorption in the sample.

Finally, the influence on the final result of uncertainties in the decay scheme parameters can be strongly reduced by basing the calculation of absolute disintegration rates on the total counting rate of all detectable radiations counted with a counter of high efficiency. The principal involved can be illustrated by an extreme example: if all radiations, including Auger electrons, conversion electrons, and L, M, N, etc X-rays, are detected in a 4π counter, which "sums" radiations emitted in coincidence, the disintegration rate is equal to the total counting rate, regardless of the details of the decay scheme. Even if the efficiency of the counter is somewhat less than 100 percent, the emission of radiations in cascade enhances the probability of a disintegration being detected. In the present work Au^{195} has been counted with a counter of 90 percent efficiency for all radiations except electrons and L, M, N, ... X-rays, for which the efficiency is zero. The disintegration rate is given to a very close approximation by

$$\lambda N = \frac{R_{total}}{1-A-0.1B} \qquad \text{(III.10)}$$

where: A is the probability of a disintegration yielding no detec-

     table radiations, and

     B is the probability of a disintegration giving one detec-

     table radiation.

The values of A and B are easily determined by an extension of the calculations leading to equations (III.7) and (III.8), and the calculated disintegration rate is only slightly influenced by uncertainties in the decay scheme. The method becomes more complicated if there are gamma rays present whose energy is so high that they have an appreciable chance of escaping from the counter. In the present work this high efficiency counting method was applied mainly to Au^{195}, whose highest gamma ray energy is 130 kev, and the complication does not arise. The method was ideal for Au^{195} for another reason: because of the long half-life of Au^{195}, the disintegration rates were low and the high efficiency enhanced the observed counting rates.

IV

EXPERIMENTAL MEASUREMENTS AND RESULTS

1. Introduction

Cross sections have been measured for the (p,pn), (p,p2n), and (p,p3n) reactions induced in gold by incident protons with energies from the reaction thresholds to 86 Mev. Gold was chosen for the target because it is a mono-isotopic heavy element, with reaction products suitable for activation measurements. (see Figure 2). Furthermore, contaminating activities from (p,xn) reactions can be removed rapidly by the distillation methods already described.

Radio-activities due to (p,p4n), (p,p5n) and (p,p6n) reactions were observed, but no cross sections have been determined. Isolation of these activities from the others that are present is difficult, and genetic relationships would require that the "fast" mercury removal technique described earlier (SectionIII.3) be very fast indeed.

Twenty-nine bombardments were performed. Mercury was removed from the first ten samples by the "slow" removal method, and so each sample yielded cross section values for only the (p,pn) and (p,p3n) reactions. This series of bombardments covered the proton energy range from 18 to 62 Mev. Each sample from the final

series of 19 bombardments gave cross section values for the (p,pn),
(p,p2n) and (p,p3n) reactions for proton energies from about 23 to
86 Mev.

2. (p,pxn) Cross Section Measurements

(a) (p,pn) Reaction

Cross section results for the reaction $Au^{197}(p,pn)Au^{196}$
are based on measured counting rates for gamma rays which follow
electron capture and β^- decay of Au^{196}. The Au^{196} decay scheme
used in the computation of disintegration rates is due to Thieme
and Bleuler[41], and it is shown in Figure 6. As seen with a
sodium iodide counter, the two gamma rays with energies of 331
and 354 kev appear as a single peak, and the gamma ray of 426
kev is just resolved from them. The gamma ray spectrum is shown
in Figure 7. Cross sections are based on the total counting rate
due to the three gamma ray transitions.

Thieme and Bleuler have measured the conversion coef-
ficients for the 331 and 354 kev transitions in Pt^{196}. They give
0.079 ± 0.008 and 0.060 ± 0.004 for the fraction of the transitions
that are internally converted, for the 331 and 354 kev transitions
respectively. Stähelin[42] has measured L- and M-shell conversion
coefficients for the 426 kev transition in Hg^{196} and finds them
consistent with multipolarity E2. Rose's tables[39] give a total
conversion coefficient of 0.04 for such a transition.

Fig. 6. Decay scheme of Au^{196} (from reference (41)).
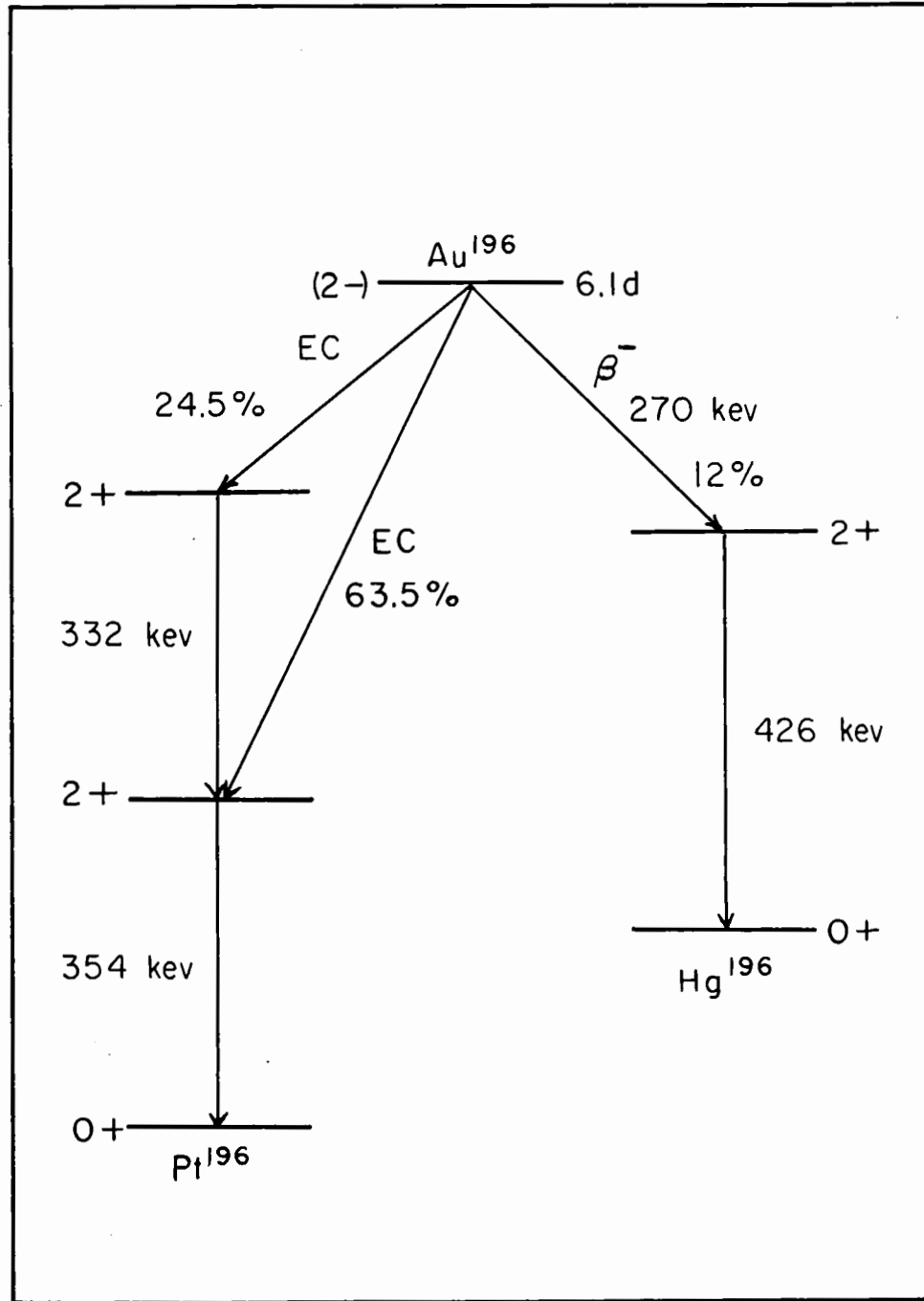
Figure 6

Fig. 7. Pulse height spectrum of gamma radiation resulting from the decay of Au^{196}, detected by a sodium iodide scintillation counter (crystal size 1 1/2 inches by 1 inch).
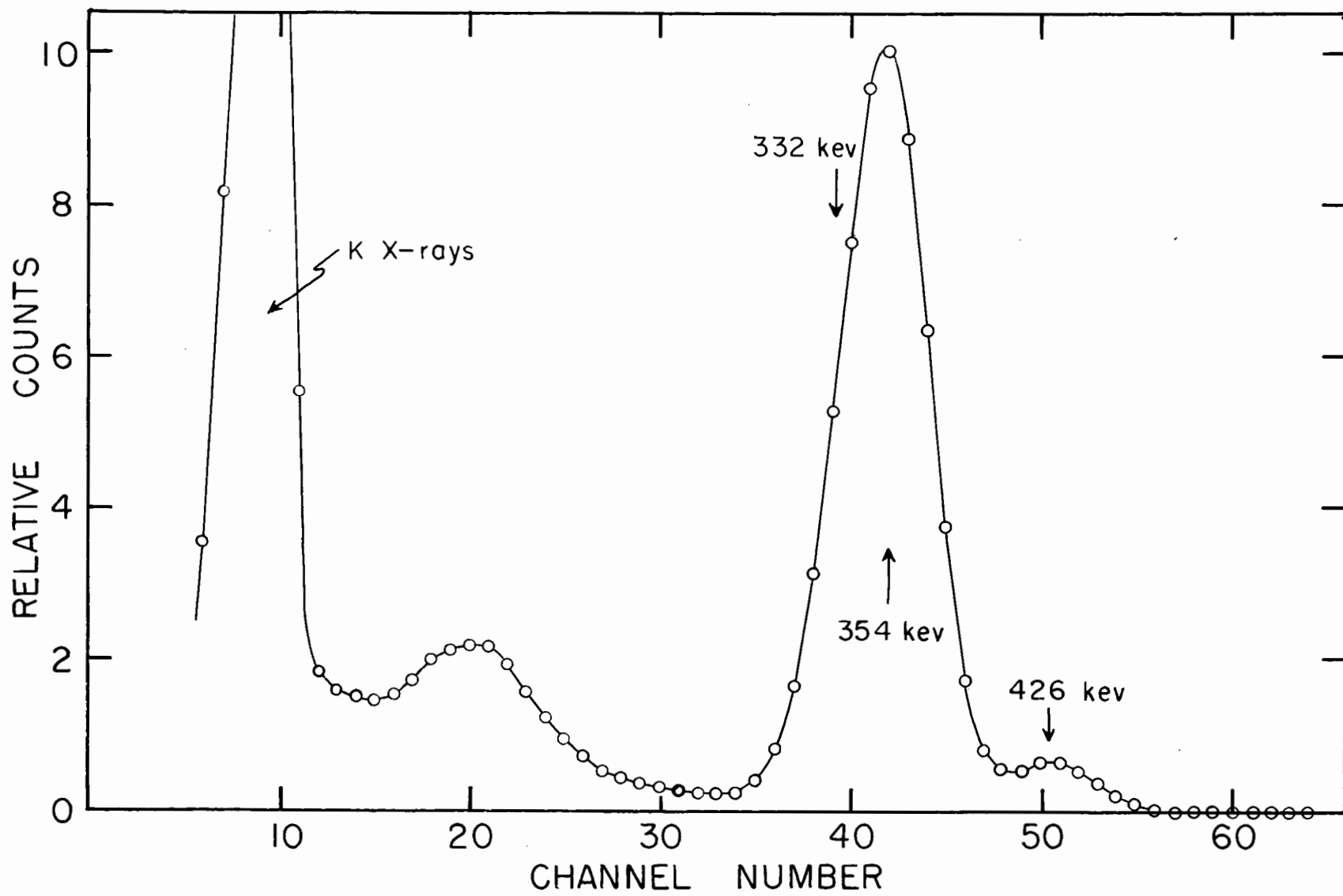
Figure 7

These conversion coefficients and the branching ratios of Thieme and Bleuler lead to a calculated total of 1.17 gamma rays per nuclear disintegration. The efficiency of the counter was taken as the mean of those for the three gamma ray energies, weighted according to their relative intensities.

A decay curve of the Au^{196} gamma ray activity is shown as the lower curve in Figure 8. The half-life found in the present work is in excellent agreement with the value of 6.10 ± 0.02 days reported by Yule and Turkevich[30]. The decay curve in Figure 8 is for a sample bombarded at 28 Mev, and consequently the gamma ray decay is free of interfering activities. At higher bombarding energies the decay curve becomes a composite one, with short-lived components due to the presence of 39 hour Au^{194}, 17.5 hour Au^{193}, 4.8 hour Au^{192}, and 3 hour Au^{191}. (see Figure 15).

Wilkinson[43] has reported a 14 hour isomeric state in Au^{196}, and it is expected that at energies above the centrifugal barrier a considerable proportion of the (p,pn) reactions will go via this state. (The statistical model predicts that the ratio of the cross sections for formation of the isomeric and ground states should approach the ratio of the statistical weights of their respective spins, at high bombarding energies. The angular momentum of the isomeric state will presumably be several units greater than that of the ground state). Evidence of formation of the isomeric state is seen in the X-ray decay curve also shown in Figure 8. (In addition to the short lived component, the presence

Fig. 8. Decay curves of gold activity in a gold sample bombarded with 28 Mev protons. The 6.1 day gamma ray activity is due to Au^{196}, and the X-ray curve contains components from 9.5 hour Au^{196m}, 6.1 day Au^{196} and 188 day Au^{195}.

Figure 8   50a
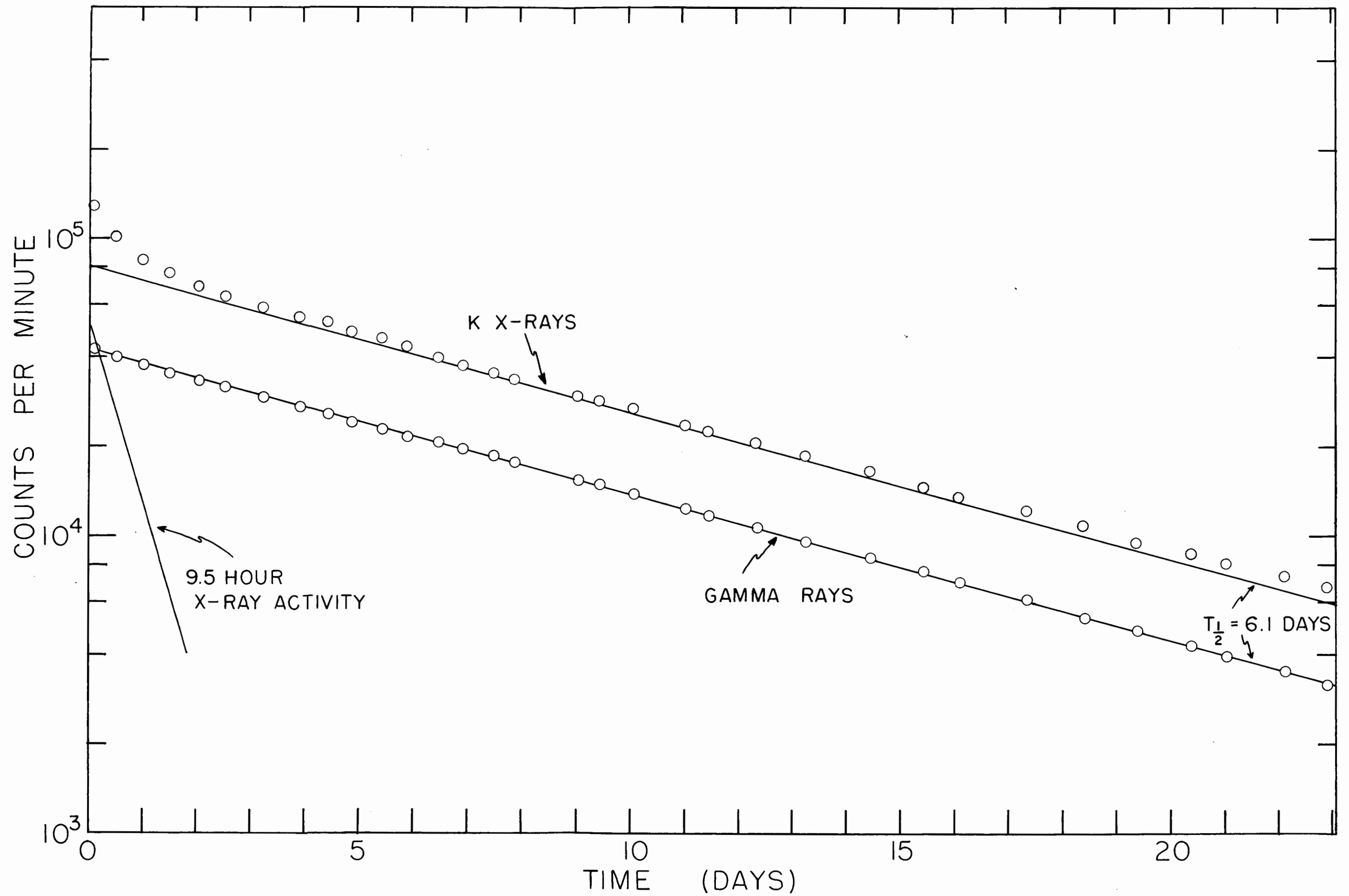
of 188 day Au^{195} is indicated). It is difficult to account for

(p,pn) reactions leading to the isomeric state by observation of

the decay of the isomer, particularly at higher bombarding energies

where other short-lived activities are formed. In the present work

cross sections were based on the 6.1 day ground state decay, and it

will be shown that the error introduced is small, if for purposes

of calculation, all reactions are considered to proceed directly

to the ground state.

We will assume, for illustration, that a fraction f of

the (p,pn) reactions lead to formation of the isomeric state, that

the electron capture branching ratio is ε, and that cross sections

are to be calculated from the ground state activity, measured after

the disappearance of the short-lived activity and extrapolated back

to zero time. If the decay constants for the isomeric and ground

states respectively are λ_1, and λ_2, then the ratio of the apparent

(p,pn) cross section to the true cross section is given by:

$$\sigma a/\sigma_T = 1 + f(\lambda_2 - \varepsilon\lambda_1)/(\lambda_1 - \lambda_2) \qquad \text{(IV.1)}$$

Measurements described in the Appendix give a value of 9.5 hours

for the half-life of the isomeric state, and equation (IV.1) reduces

to

$$\sigma a/\sigma_T = 1 + f(0.07 - 1.07\varepsilon) \qquad \text{(IV.2)}$$

It is seen that if there is no electron capture branch the apparent

cross section will be at most 7 percent high, and since f is considerably less than unity, the actual error will be small. (The present experiments indicate that f is about 0.1 for 30 Mev bombarding energy. For higher energies other short-lived activities make such an evaluation difficult. Probably f is less than 0.5 for all bombarding energies considered here.) The error decreases as ε increases, and becomes zero for an electron capture branching ratio of 7 percent. The apparent cross section is low for ε greater than 7 percent, but the error will not be serious for ε less than 20 percent.

An estimate of the electron capture branching ratio can be made from an examination of the decay curve of the ground state gamma rays shown in Figure 8. Electron capture events in the isomeric state would give rise to a short-lived component in the decay curve, since the two 2+ states shown for Pt^{196} in Figure 6 must be populated either directly or indirectly by electron capture in the high spin isomeric state. The fact that the decay curve shows a pure 6.1 day decay indicates that the electron capture probability is not large. The short-lived component in the K X-ray decay curve shown in Figure 8 is due to K conversion of the isomeric transitions. It is emphasized that this analysis is not very sensitive, since a 7 percent capture branch must necessarily lead to a pure 6.1 day gamma ray decay, due to the cancelling effect of the ground state growth resulting from isomeric transitions; for an electron capture branch of less than 7 percent the ground state

activity will grow, but the growth would not be observable due to experimental errors in the decay curves. However, the electron capture branching ratio is indicated to be less than 20 percent.

An extensive investigation of the decay scheme of the Au^{196} isomeric state was carried out in connection with this work, and the results are presented in the Appendix. A small electron capture branch was observed, and the branching ratio has been estimated to be less than 10 percent. The Au^{196m} decay scheme was investigated concurrently by Van Lieshout et al, and their results have recently been published[44]. Their experiments indicate that the isomeric state decays entirely by an isomeric transition, but the weak conversion electron lines attributed in the present experiments to electron capture events would probably not be resolved in their measurements. The Van Lieshout results support the conclusion that the capture probability is small.

It is estimated that reactions leading to the isomeric state of Au^{196} cause an uncertainty of about 3 percent in the measured (p,pn) cross section.

The (p,pn) cross section results are summarized in Table I and are shown graphically in Figure 9. Also shown in Figure 9 are low energy cross section values from the work of Sosniak[29] (multiplied by 2 to correct an error in beam monitoring) and the lowest energy point from the high energy results of Yule and Turkevich[30].

Fig. 9. Cross section of the reaction Au^{197} (p,pn)Au^{196} as a function of incident proton energy. The circles are from the present work, the crosses from Sosniak[29] and the triangle from the work of Yule and Turkevich[30]. The error bar represents the estimated standard error in the absolute cross section values.
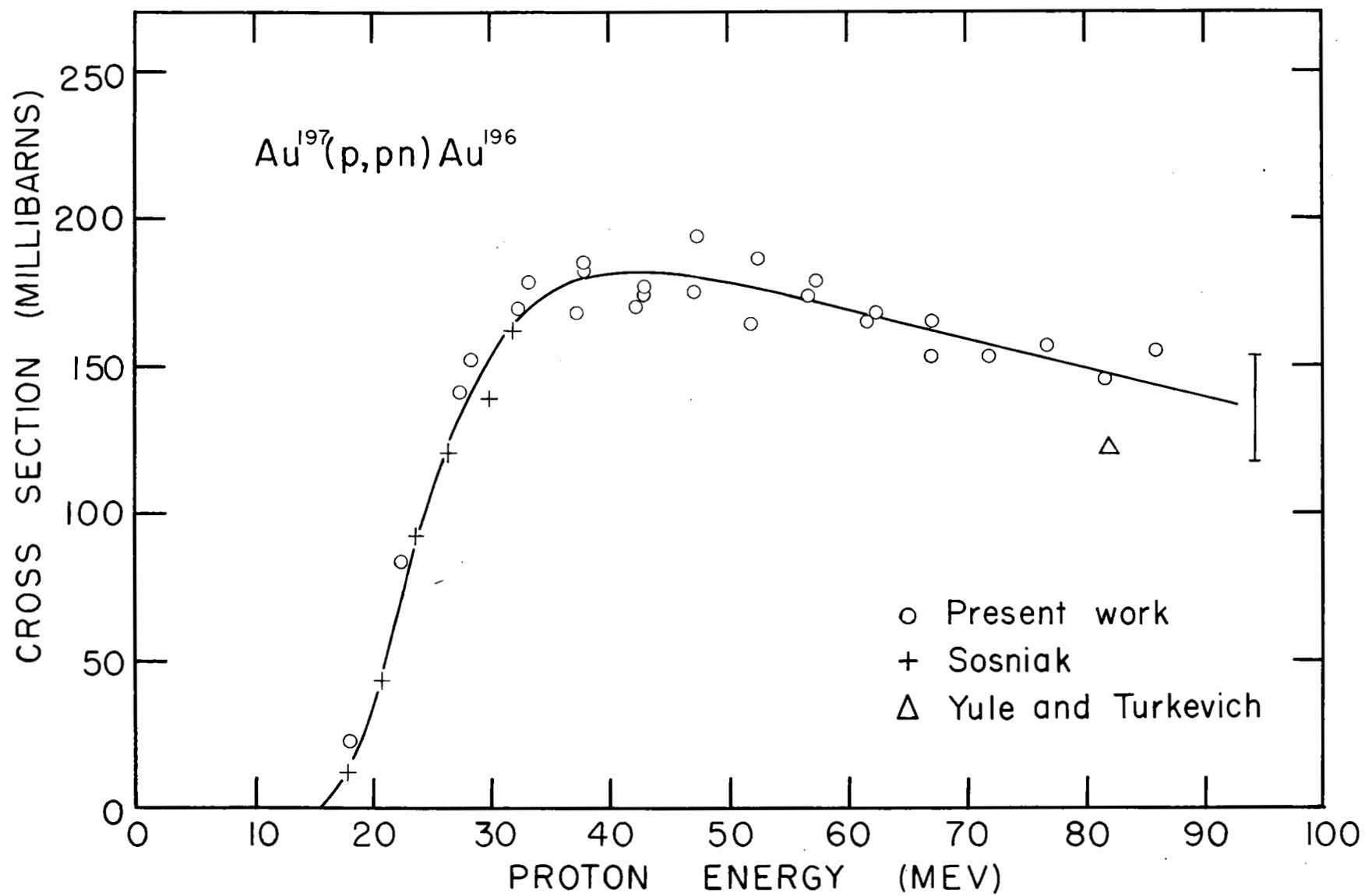
$Au^{197}(p,pn)Au^{196}$

o   Present work
+   Sosniak
△   Yule and Turkevich

CROSS SECTION (MILLIBARNS)

PROTON   ENERGY   (MEV)

Figure 9

54a

(b)   (p,p2n) Reaction

. The (p,p2n) reaction in Au^{197} leads to 188 day Au^{195}. The decay scheme for this nuclide is shown in Figure 10, and is essentially that given in the tables of Strominger, Hollander and Seaborg[45], with branching ratios from a later paper by Bisi et al[46]. Cross sections were based on the total counting rates of K X-rays, and the 31, 99 and 130 kev gamma rays, counted with the double sodium iodide counter previously described (SectionIII.4). The pulse height spectrum, which clearly shows summing effects in the high efficiency counter, is shown in Figure 11. The estimated efficiency of the counter for all radiations is 0.90 ± 0.05. Its efficiency for counting Au^{195} disintegrations is estimated as follows.

Bisi and his co-workers have determined the ratio of total capture to K-capture for decays to the 130 kev level in Pt^{195} by detecting coincidences between K X-rays and 130 kev gamma rays. They report a value of 6.5 ± 0.9 and use the results of Brysk and Rose[37] to calculate the transition energy, and hence the total to K-capture ratio for the other branch. This gives a value of total to K-capture of 1.49 for decays to the 99 kev level. Conversion coefficients for the 31 kev and 99 kev transitions are also given. The conversion coefficients for the weak 130 kev transition were determined from the tables of Rose[39], assuming the transition to be pure E2. The ratio of cross-over to cascade

Fig. 10. Decay scheme of Au^{195} (from references (45) and (46)).

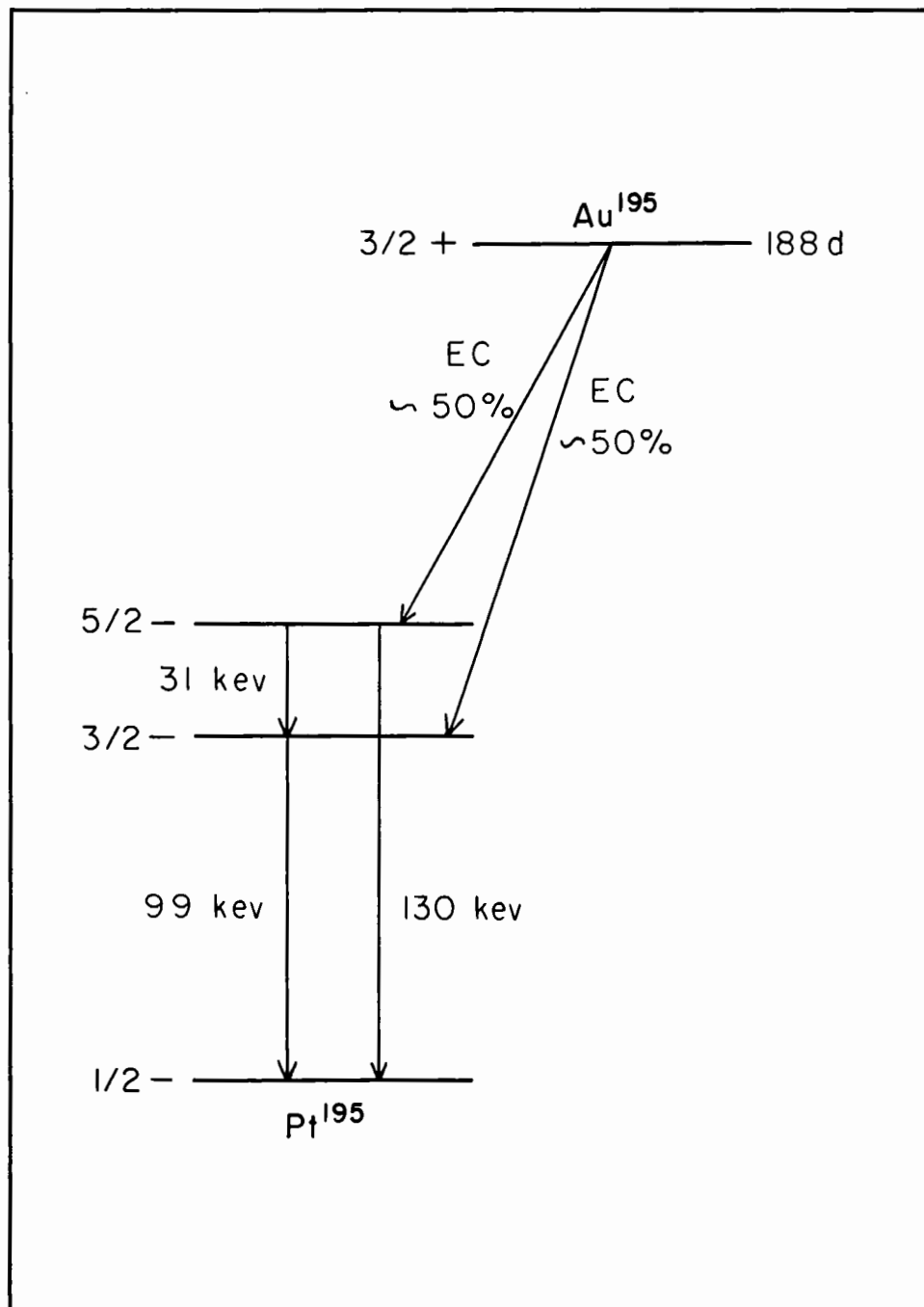Figure 10   56a

Fig. 11. Pulse height spectrum from Au^{195} radiations detected by a NaI(Tl) scintillation crystal with 95 percent geometrical efficiency (see text). Radiations emitted in coincidence result in the "sum" peaks indicated on the diagram. The radiations and "sum" events designated in brackets on the figure are relatively very weak.
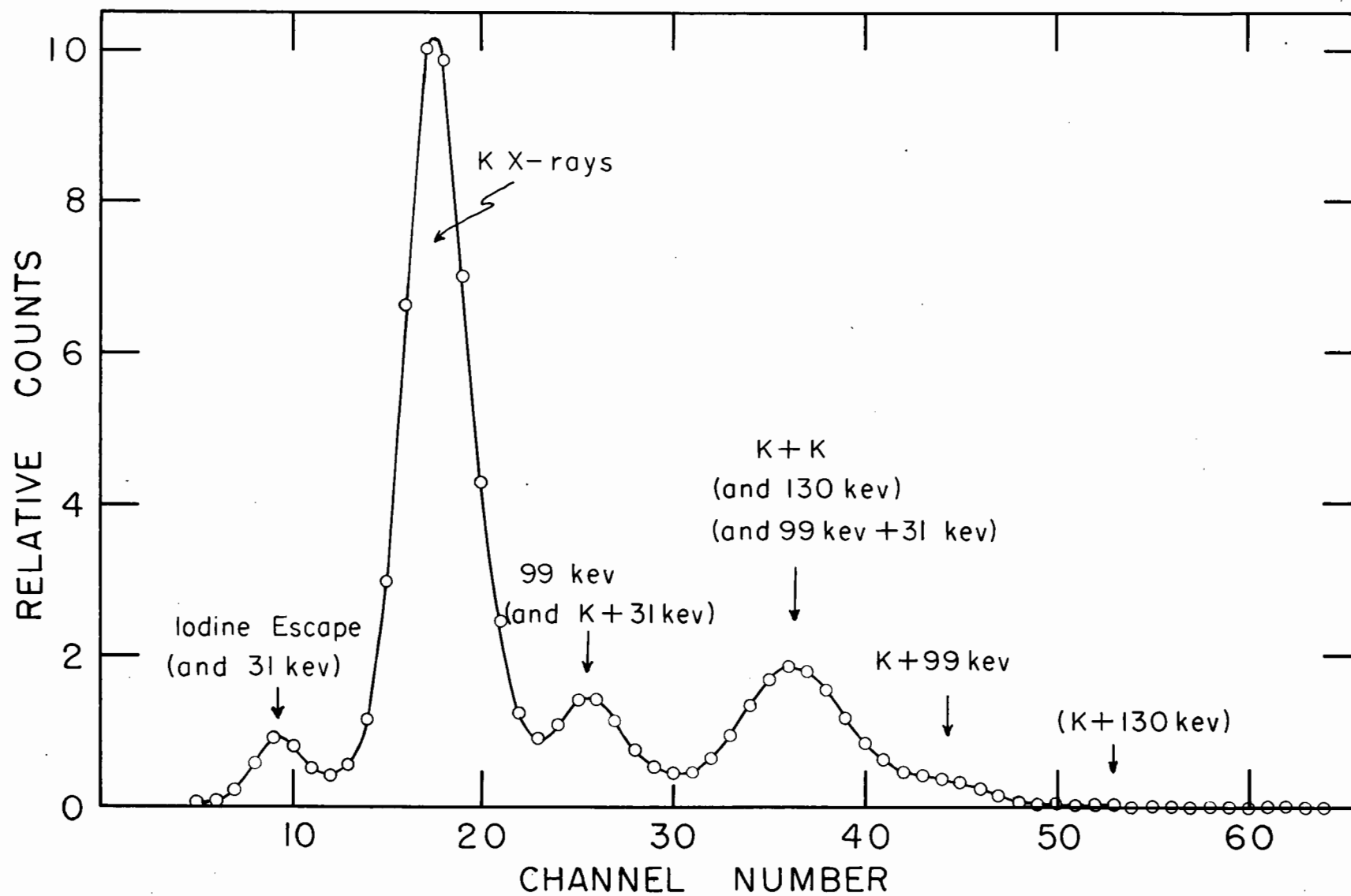
Figure 11

57a

decay of the upper level in Pt^{195} was calculated from the relative intensities of 99 and 130 kev gamma rays given by Bisi et al, and the conversion coefficients mentioned above.

A calculation of the type outlined in Section (III.5b) based on the above information, gives a counting efficiency of 81 percent. That is, there will be 0.81 recorded counts, including sum counts, per nuclear disintegration. This efficiency factor is extremely insensitive to errors in the decay scheme parameters used. For example, the use of electron capture branching ratios of 35 percent and 65 percent for the upper and lower branches respectively, as given by de Shalit et al[47] introduces an error of 2 percent into the final result. The assumption of a 20 percent electron capture branch to the ground state introduces 7 percent error. (The results of Bisi et al are consistent with no ground state branching. Single crystal coincidence results from the present work support such an assumption). The total capture to K-capture ratio for the upper branch can be in error by 50 percent without changing the calculated efficiency by more than 1 percent, and the results are only slightly more dependent on the capture ratio for the other branch. An uncertainty of 2 percent results from 10 percent uncertainty in conversion coefficients for the 99 kev transition, and errors in the other conversion coefficients are much less important. The ratio of cross-over probability to cascade probability in decay of the 130 kev level can be in error by a factor

of 4 without affecting the cross section results by more than 1 percent. Finally, the 5 percent uncertainty assumed for the efficiency of the counter itself introduces an uncertainty of less than 3 percent in the final results. An over-all standard error of 5 percent has been assumed in the calculated absolute disintegration rates.

The long-lived Au^{195} activity was counted for a period of 40 days, commencing for the different samples from 50 to 100 days after bombardment. This allowed adequate time for the decay of 6.1 day Au^{196}, and the small amount of 11 day Ir^{189} detected earlier in some of the samples bombarded at high energies. (This Ir^{189} comes from the decay chain $Hg^{189} \rightarrow Au^{189} \rightarrow Pt^{189} \rightarrow Ir^{189}$). The gamma ray spectrum indicated the presence of no other interfering activities. A half-life of 188 days was assumed for cross section calculations; this is an average of the values 185 ± 5 days reported by Wilkinson[43], and 192 ± 5 days given by Bisi et al[46]. A composite decay curve showing the decay of shorter lived K X-ray activity is presented in Figure 12.

The (p,p2n) cross section results are summarized in Table I, and are shown in Figure 13.

(c) (p,p3n) Reaction

This reaction leads to the formation of 39 hour Au^{194}, and cross section determinations have been based on measurements of both K X-rays and gamma rays. The rather complex level scheme of Au^{194}

Fig. 12. Decay curve of gold gamma ray and X-ray activity in a gold sample bombarded with 67 Mev protons. The 188 day component is due to Au^{195}, the 6.1 day component to Au^{196} and the 39 hour component is due to Au^{194}; short-lived activities due to Au^{193}, Au^{192} and Au^{191} are indicated.
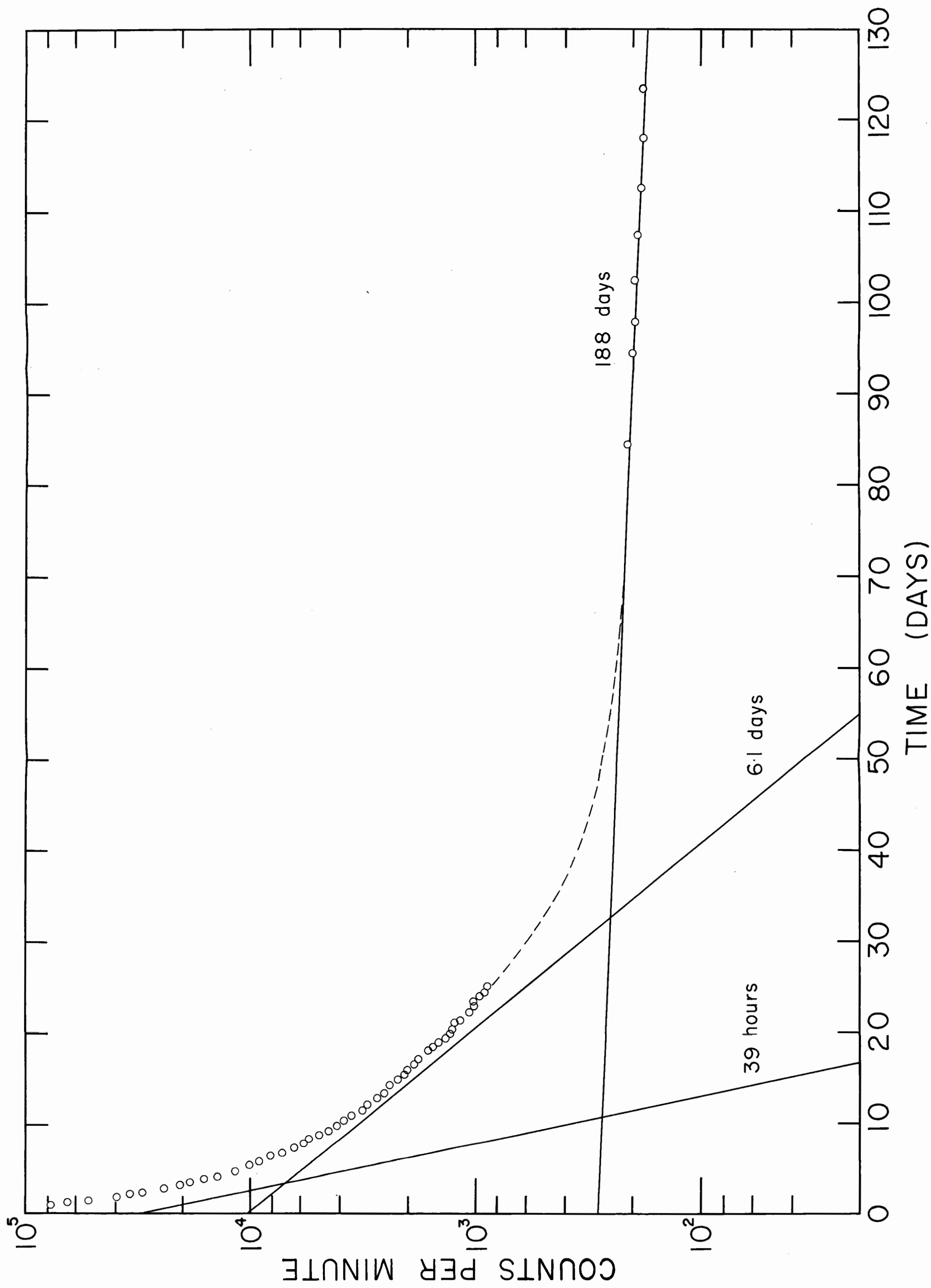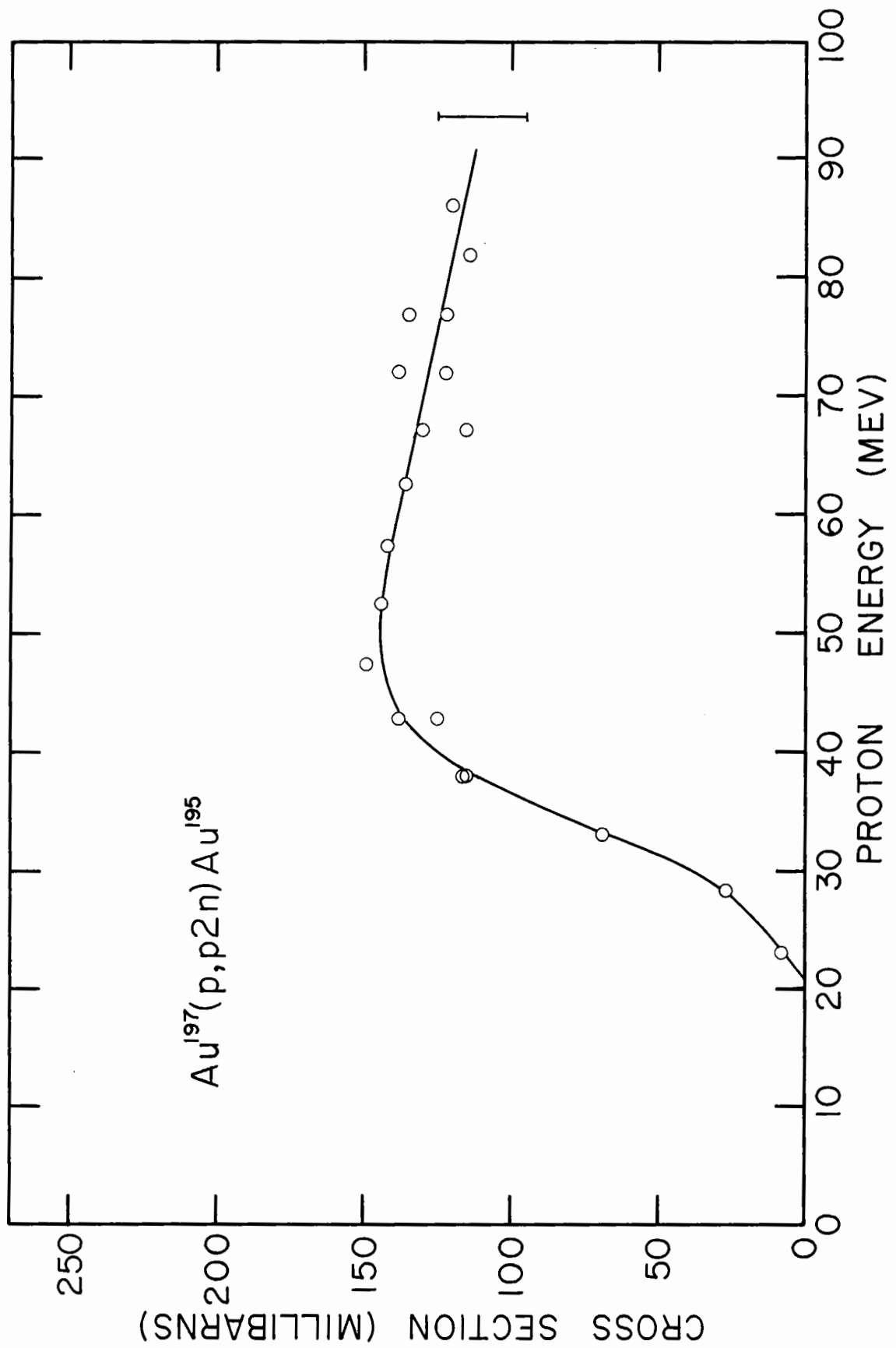
Figure 12

Fig. 13. Cross section of the reaction Au^{197} (p,p2n)Au^{195} as a function of incident proton energy. The error bar indicates the estimated standard error in the absolute cross section values.

Figure 13   61a

Figure 13

$Au^{197}(p,p2n)Au^{195}$

CROSS SECTION (MILLIBARNS)

PROTON ENERGY (MEV)

has been investigated by Thieme and Bleuler[48], and it is repre-
sented in Figure 14. The relative intensities of the various gamma
rays are given by these authors.

The gamma ray spectrum consists of intense 291 and 327
kev components and several weaker gamma rays of higher energies.
The 291 and 327 kev gamma rays can be counted conveniently, but
absolute disintegration rates cannot be calculated from these
measurements since the electron capture branching ratios are not
known. K X-ray counting, on the other hand, has the disadvantage
that at higher energies K X-rays from 17.5 hour Au^{193} and, to a
lesser extent, from 3.0 day Pt^{191} interfere, since they cannot
be separated from the gross X-ray decay curve. The gamma rays
were used as an indicator of the relative cross sections, and the
results so obtained were normalized to the absolute values measured
by K X-ray counting at energies below the $Au^{197}(p,p4n)Au^{193}$ threshold.

The 291 and 327 kev gamma rays appear in the sodium iodide
scintillation spectrum as a broadening of the total energy peak from
the Au^{196} gamma radiations, and they are easily separated from the
gross decay curve. The 17.5 hour Au^{193} activity mentioned above
causes little difficulty since only about 0.08 gamma rays per dis-
integration are unresolved from the Au^{194} photopeak[45]. (This is
to be compared with about 10 times as many 291 or 327 kev gamma rays
per decay of Au^{194}). The interfering gamma rays from Pt^{191} are of
low intensity, and for the three highest energy bombardments a
correction of about 5 percent was made, based on measurement of

FIGURE 14 .   .

Figure 14   63a
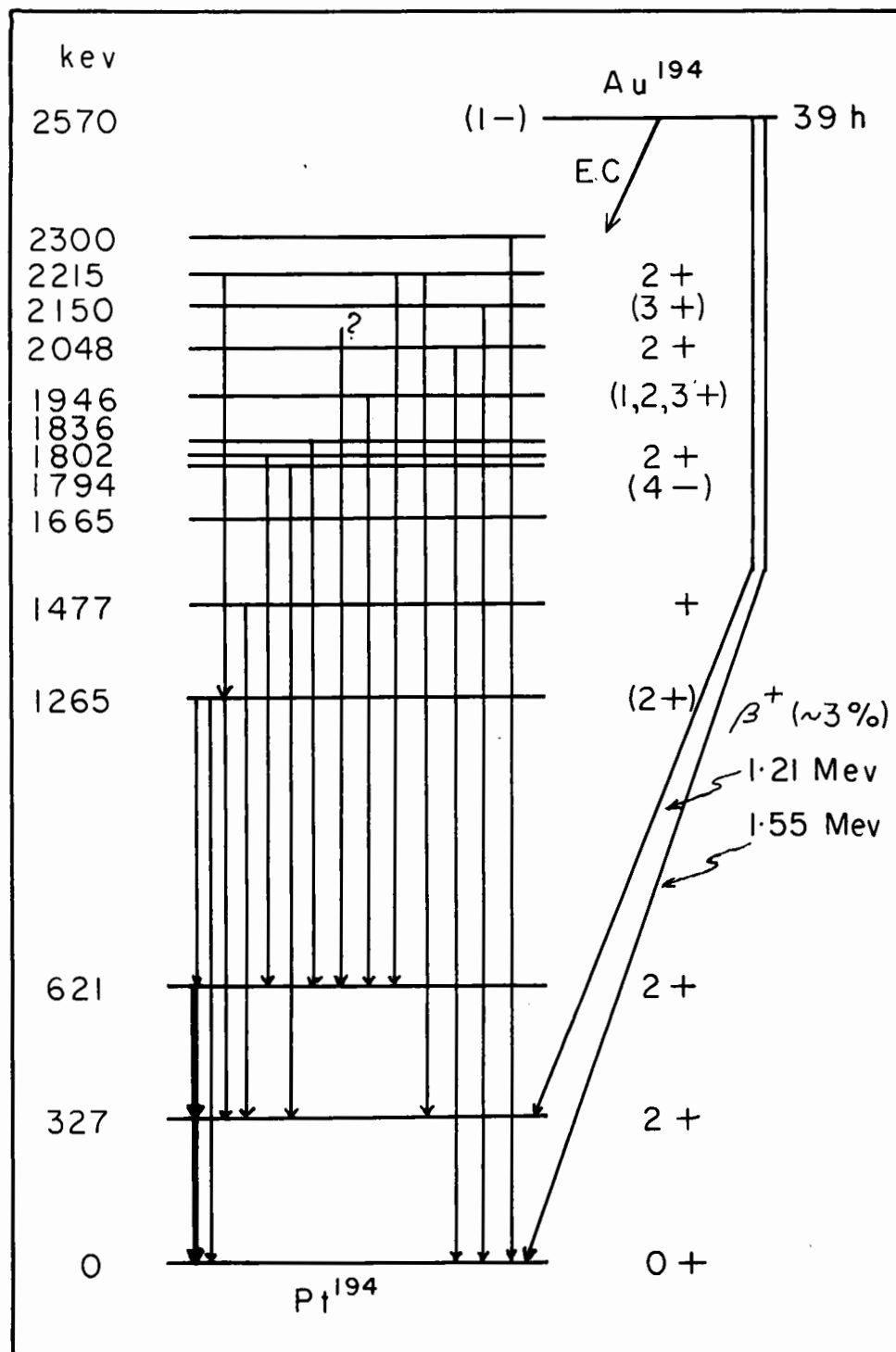
the counting rate of a 530 kev component whose intensity relative to that of the interfering gamma rays is known[45].

A composite decay curve showing gamma ray activity from Au^{194} is shown in Figure 15. This curve is for a sample bombarded at 67 Mev, and short-lived activities due to Au^{193}, Au^{192} and Au^{191} are in evidence.

The small (about 3 percent) positron decay branch establishes the transition energies for electron capture events, and according to Thieme and Bleuler most of the transitions are ordinary first forbidden. The calculated value of the total capture to K-capture ratio is 1.35 ± 0.07. This value is based on an average of ratios for each of the transitions, weighted according to rough branching ratios determined from relative gamma ray intensities. The transition probability for electron capture to the ground state relative to the first excited state was based on the relative positron branching to these states, and the theoretical ratio of K-capture and positron decay probabilities[37][49]. The total to K-capture ratio is quite insensitive to uncertainties in the branching ratios since for the majority of the transitions the disintegration energy is large compared to the K-electron binding energy. The contribution of K X-rays from internal conversion has been determined from experimental conversion coefficients given by Thieme and Bleuler, and the calculated branching ratios. The correction amounts to 5 percent. The (p,p3n) cross section results are shown in Table I and Figure 16.

Fig. 15. Decay curve of gold gamma ray activity in a gold sample bombarded with 67 Mev protons. The open circles are experimental points, and the solid circles and triangles result from successive subtractions from the gross decay curve. The 6.1 day component is due to Au^{196} and the 39 hour component to Au^{194}; short-lived components due to 17.5 hour Au^{193}, 4.8 hour Au^{192} and 3 hour Au^{191} are in evidence.

Figure 15   65a
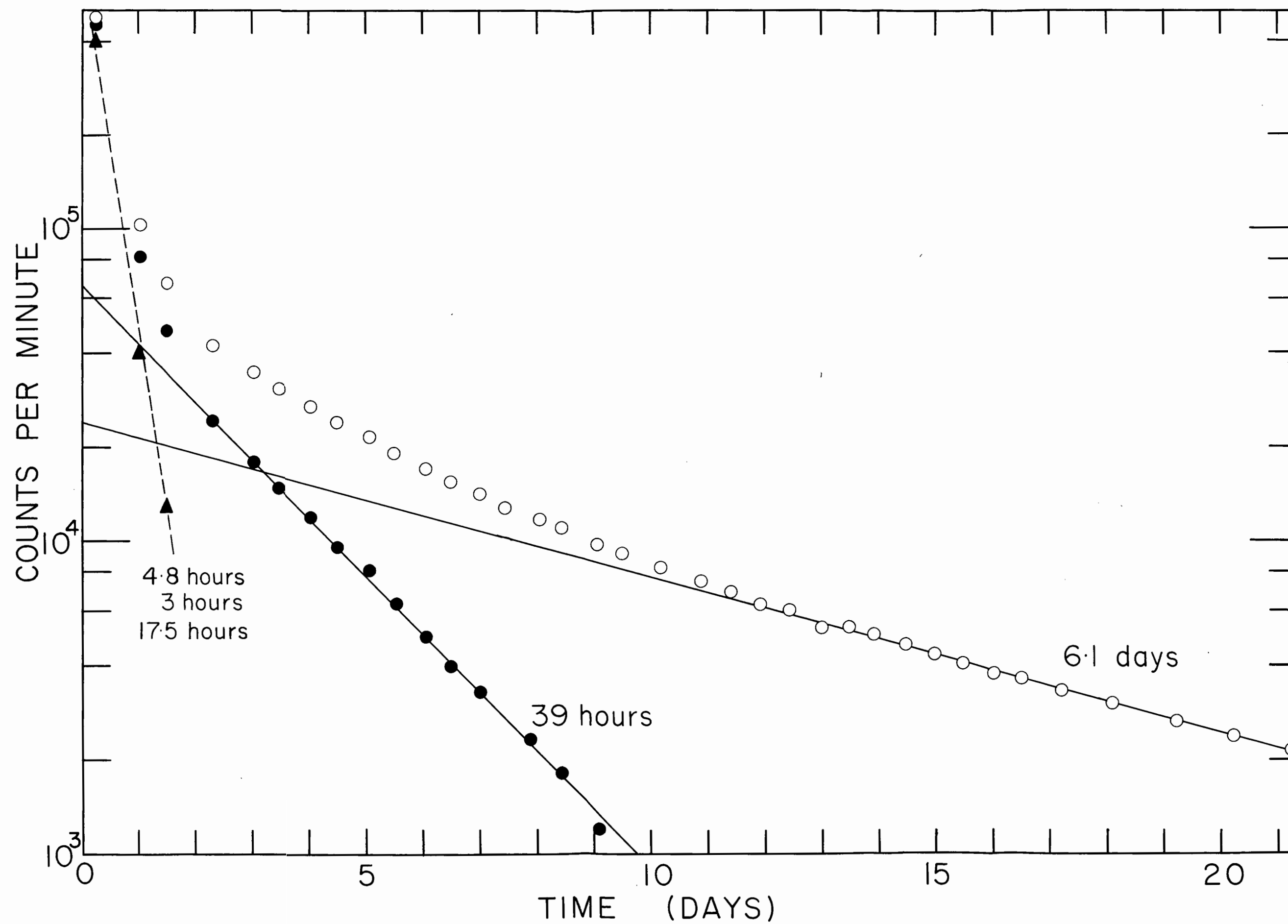
Fig. 16. Cross section of the reaction Au^{197}
(p,p3n)Au^{194}, as a function of incident proton energy.
The error bar indicates the estimated standard error
in the absolute cross section values.

Figure 16   66a

Au^{197}(p,p3n) Au^{194}
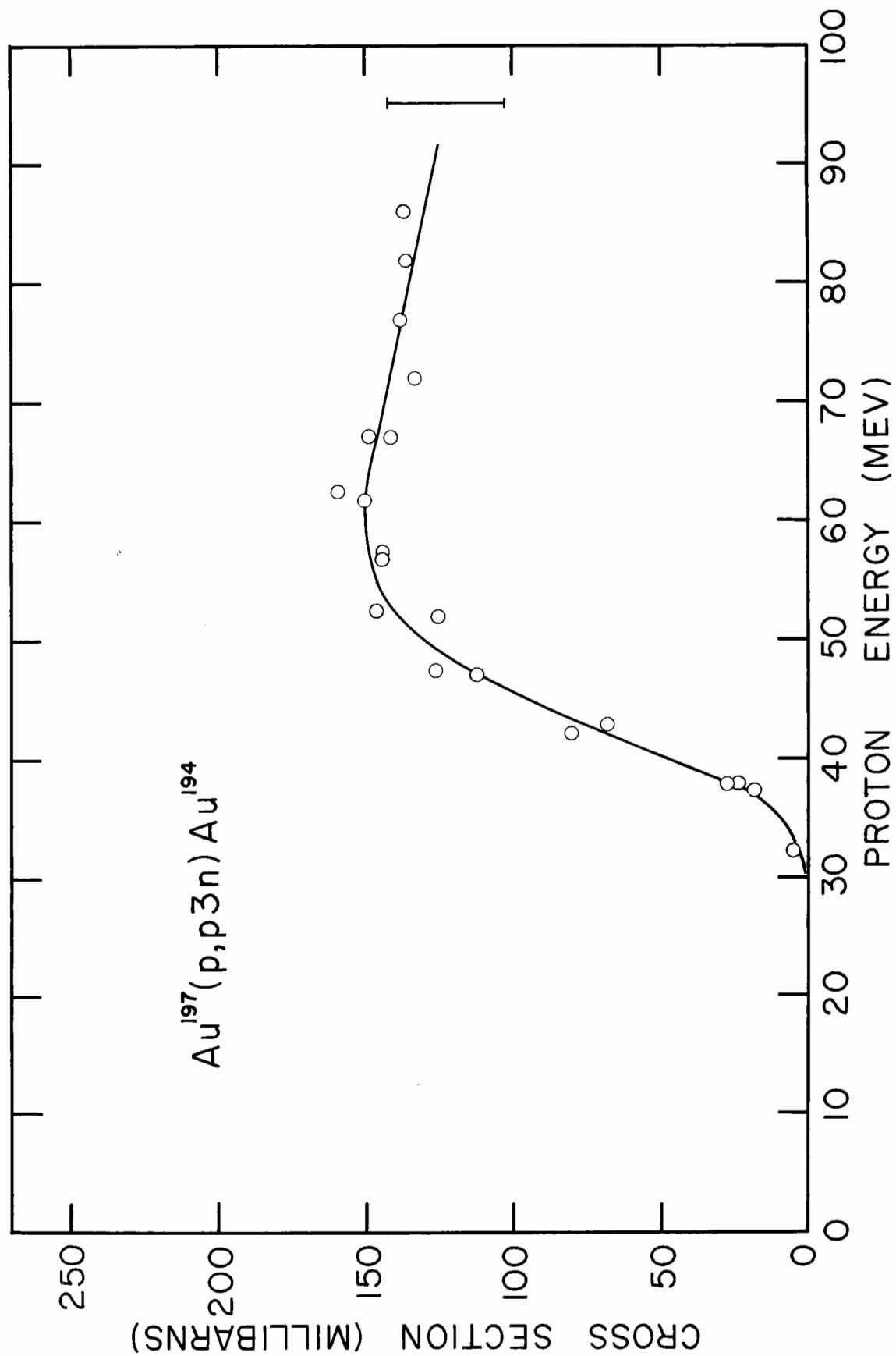
TABLE I

Experimental Au^{197}(p,pxn) Cross Section Results

Proton Energy (Mev)	(p,pxn) Cross Sections (mb)		
	(p,pn)	(p,p2n)	(p,p3n)
18.0	23.6		
22.3	83.3		
23.2		8.1	
27.5	141		
28.3	152	26.8	
32.4	169		6
33.2	178	69	
37.3	168		18
37.9	182	116	27
	185	115	24
42.2	170		80
42.8	174	125	68
	177	138	
47.2	175		112
47.4	194	149	126
51.9	164		125
52.5	186	144	146
56.8	174		144
57.4	179	142	144
61.7	165		150
62.5	168	136	159
67.1	153	115	149
	165	130	141
72.0	153	138	133
		122	
76.9	157	135	138
		122	
81.8	146	114	136
86.0	155	120	137

3. Experimental Errors

Table II shows the factors entering into the measurement of the (p,pxn) cross sections, with their estimated individual standard errors.

Table II

Entry Number	Factor	Standard Error %
1	Gold sample thickness	2
2	Decay curve analysis	5
3	Errors in beam monitoring not including the absolute value of the monitor cross section	5
4	Monitor cross section	7
5	Scintillation counter efficiency	7
6	Determination of number of photons emitted per disintegration	6

From Table II we may compute three kinds of standard error for the cross section measurements, compounding the errors in the usual way.

(a) Relative errors among the measured points for a single (p,pxn) curve: Here all factors except 6 enter, and the other factors must be reduced. Factor 4 is taken to be 5 percent and the others were

arbitrarily reduced to 3 percent to give a standard error of 7 percent, consistent with the scatter of the experimental cross section points about a smooth curve.

(b) Error in relative cross sections for different (p,pxn) reactions at a particular energy: Here we include all factors except 4, and the result is 12 percent.

(c) Error in absolute cross sections: All factors are included in this estimate giving a standard error of 13.5 percent.

There may be departure from these error estimates in certain instances. For example, in the case of the (p,pn) reaction factor 2 is probably overestimated, particularly in the later runs when the digital 256-channel kicksorter was used. The error in this same factor is likely larger than 5 percent for the (p,p3n) measurements since here cross sections were based on a short-lived component in a complex decay curve. For these same measurements factor 6 is probably at least 10 percent due to uncertainty in the normalization of gamma ray activity to K X-ray activity. An uncertainty of about 2 Mev in the energy of the incident protons causes additional uncertainty in the regions of rapidly rising (p,pxn) cross sections, and this same uncertainty in energy makes the beam monitoring less reliable below 30 Mev, where the C^{12}(p,pn) cross section varies rapidly. Finally, an additional uncertainty of 3 percent results, in the case of the (p,pn) cross section, from

reactions leading to the isomeric state of Au^{196}.

The estimated standard errors in the absolute cross section values are indicated by the error bars shown in Figures 9, 13 and 16.

4. Discussion of Cross Section Results

(a) (p,pxn) Cross Sections

The experimental cross section results for the (p,pn), (p,p2n) and (p,p3n) reactions have been shown in Figures 9, 13 and 16. The smooth curves drawn through the experimental points in these figures are presented together in Figure 17, and the sum of the 3 cross section curves is also shown.

The (p,pn) cross section rises from a threshold at about 16 Mev and has a peak cross section of 180 millibarns at 40 Mev. The cross section then decreases slowly for increasing bombarding energy. The results of the present measurements are in good agreement with the work of Sosniak[29]. The cross section at 82 Mev is about 20 percent higher than the value reported by Yule and Turkevich[30]; however this disparity is only slightly greater than the combined standard errors for the two measurements.

The (p,p2n) cross section has a threshold at about 21 Mev and rises more slowly than the (p,pn) curve to a peak value of 145 millibarns for 50 Mev incident protons. The cross section

Fig. 17. Cross sections of (p,pn), (p,p2n) and (p,p3n) reactions from the present work are represented by the solid curves, and the circles represent the sum of these cross sections. The dashed curve is a theoretical one based on the statistical model calculations of Jackson[9]. Statistical model predictions for the (p,p2n) and (p,p3n) cross sections are not shown; they are similar to that for the (p,pn) reaction, but lie 10 and 20 Mev higher on the energy scale, respectively.

Figure 17
71a

Figure 17
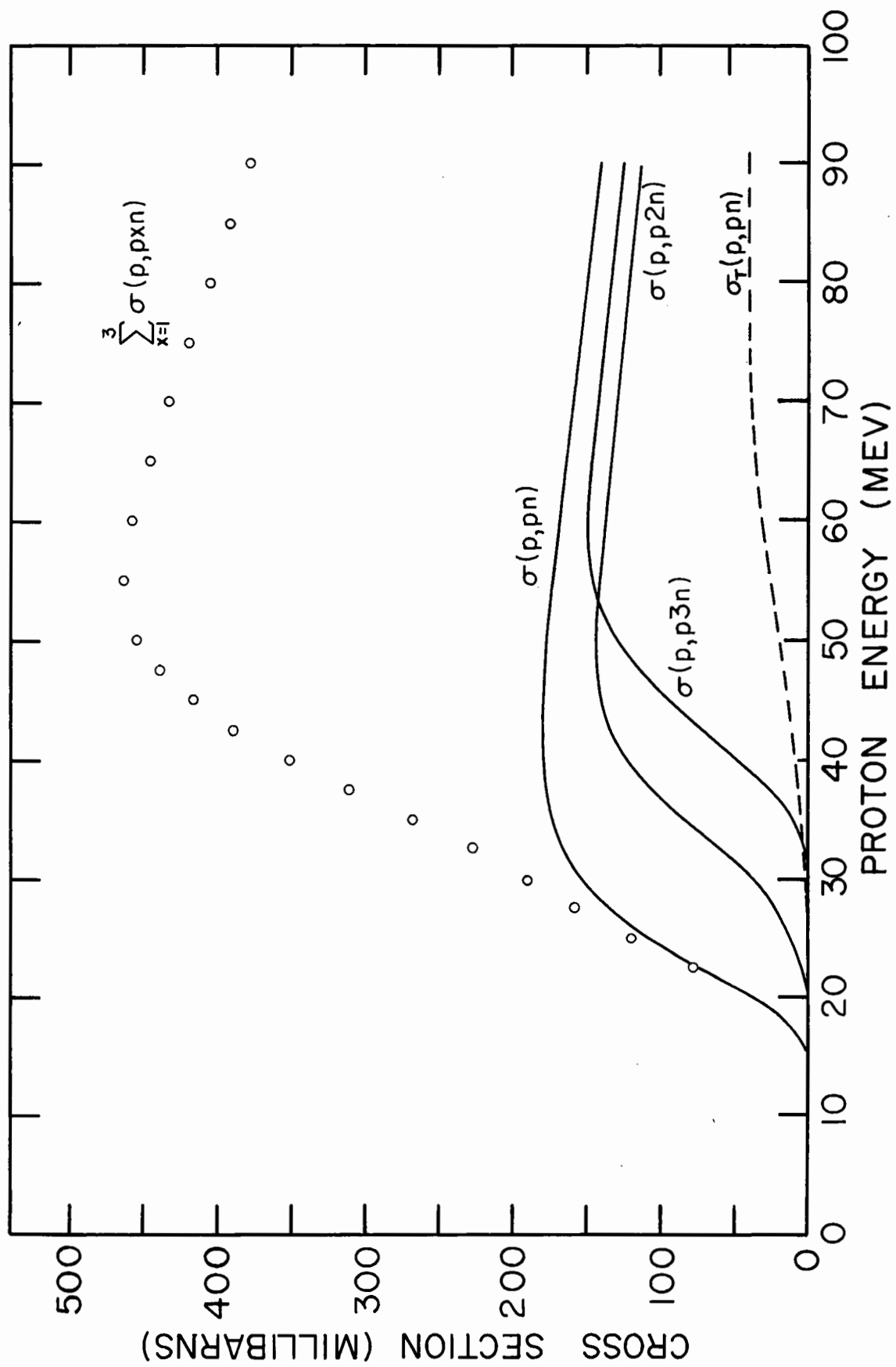
for higher bombarding energies shows an energy dependence similar to that for the (p,pn) reaction.

The (p,p3n) reaction threshold is at about 30 Mev, and the shape of the cross section curve is like that for the (p,p2n) cross section, except near the threshold where the latter rises more rapidly. The peak cross section for the (p,p3n) reaction appears to be slightly larger than for the (p,p2n) reaction, but this difference may not be real. The (p,p2n) and (p,p3n) cross sections are always lower than the (p,pn) cross section.

The (p,pxn) cross sections cannot be interpreted in terms of the statistical model. The individual (p,pxn) cross sections do not show the drop predicted by evaporation theory for bombarding energies above the threshold for the (p,p(x+1)n) reaction. Thus the emitted particles are carrying away large amounts of kinetic energy, and this is characteristic of a direct interaction. More important, the magnitudes of the (p,pxn) cross sections are much larger than the predictions of the statistical model. The (p,pn) cross section calculated from the statistical model theory of Jackson[9] is shown by the dashed curve in Figure 17. Theoretical cross sections for the (p,p2n) and (p,p3n) reactions are not shown; they are similar to that for (p,pn), but lie 10 and 20 Mev higher on the energy scale, respectively. It is seen that for bombarding energies near the peaks of the experimental curves, the theoretical cross sections are at least an order of magnitude too small.

There is convincing experimental and theoretical evidence that (p,pxn) reactions, which may be called inelastic proton scattering reactions, are due to initial two-body collisions in the diffuse edge of the nucleus (see Section II). These inelastic scattering reactions can be considered, at least for low bombarding energies, to take place in three stages:

(i) The incident proton suffers a quasi-free two-body interaction with a proton or neutron in the diffuse nuclear edge.

(ii) Either the incident particle and the struck particle both emerge from the nucleus with energies and angular distributions characteristic of direct interactions, or a proton emerges, and the other particle enters the nuclear core to form a compound nucleus.

(iii) Residual energy of excitation, from either of the processes in (ii), can cause neutron evaporation.

At higher bombarding energies, where the nuclear edge becomes more transparent to the incident particles, internal direct interactions will be important; Jackson's calculations show that at 90 Mev about one third of the reactions can be interpreted in this way.

On the basis of the three stage reaction mechanism outlined above, it is expected that if both the particles that are involved in the initial collision enter the nuclear core, reactions

of the type (p,xn) will result. If the struck particle is a
neutron and only the incident proton is scattered into the nuc-
leus, the final result will also be a (p,xn) reaction. If both
the incident and struck particles emerge from the nucleus directly,
a (p,pn) or (p,2p) reaction results, unless the nucleus receives
sufficient excitation energy during the interaction to cause sub-
sequent neutron evaporation. Since the nuclear core subtends a
solid angle of nearly 2π steradians at the point of collision,
the direct escape of both particles is relatively unlikely. Both
particles must move in a plane that is tangential to the nuclear
core, and since the angular distribution of the two particles will
be strongly peaked forward (the momentum of the struck particle
before the collision appears to be small, and will have only a
small effect on the scattering process), both particles can emerge
only if the initial collision takes place in an equatorial band,
where the incident particle is considered to travel in a north-
south direction[25]. Similarly, interactions in which only one
particle escapes directly must take place in the same region of
the nucleus, though the band can be wider.

A qualitative interpretation of the relative magni-
tudes of the (p,pn), (p,p2n) and (p,p3n) reaction cross sections
can be given on the basis of the reaction model outlined above.
The protons emitted in these reactions are expected to have a
broad energy distribution, and Eisberg and Igo[1] have shown that

for 31 Mev incident protons, the energy spectrum of inelastically
scattered protons is relatively flat. The distribution of resi-
dual excitation energy in the nuclear core will also be relatively
flat, and at bombarding energies well above the threshold for a
particular (p,pxn) reaction, the direct emission of a proton
would be followed, with similar probability, by the evaporation
of x or x - 1 neutrons. This is consistent with the approximate
equality of the experimental (p,p2n) and (p,p3n) cross sections
for bombarding energies above 50 Mev. For energies just above a
particular (p,pxn) threshold, the (p,p(x-1)n) reaction will of
course predominate over the (p,pxn) reaction.

The (p,pn) cross section is larger than that for the
(p,p2n) and (p,p3n) reactions, and this is probably due to (p,d)
pickup reactions, which have not been distinguished in the present
experiments from true (p,pn) events. Cohen and Ruben[15] have
shown that the (p,d) cross section is 42 millibarns for 23 Mev
protons, and the experiments of Eisberg and Igo[1] indicate an
upper limit of about the same magnitude for the cross section at
31 Mev. If the (p,d) cross section remains constant or drops
slowly for increasing bombarding energy, the true (p,pn) cross
section is similar to that for the (p,p2n) and (p,p3n) reactions.
Complex pickup reactions like (p,t), (p,dn) and (p,tn) can of
course contribute to the observed (p,p2n) and (p,p3n) cross
sections, but the effect is likely small. Cohen and Rubin report
a cross section of 9.5 millibarns for the (p,t) reaction in gold

for 23 Mev protons. The (p,t) reaction, which is energetically favoured over the true (p,p2n) reaction by about 8.5 Mev, does however contribute to a lowering of the apparent threshold of the (p,p2n) + (p,t) reaction. The effect is visible at the beginning of the (p,p2n) curve in Figure 17. In the present experiments the total (p,p2n) cross section at 23.2 Mev (8.1 millibarns) is completely accounted for by the (p,t) reaction, and the fact that the experimental cross section rises slowly for energies up to the true (p,p2n) threshold indicates that the (p,t) reaction represents only a small fraction of all (p,p2n) events.

The sum of the smoothed individual (p,pxn) cross sections is shown in Figure 17. This curve rises to a peak value of about 450 millibarns at a bombarding energy of 55 Mev. The sum curve does not contain any great significance for proton energies above about 50 Mev, since (p,pxn) cross sections for $x > 3$ are not included. Eisberg and Igo have reported a cross section of 290 millibarns for the inelastic scattering of 31 Mev protons incident on gold, and a useful comparison can be made between this result, and the (p,pxn) sum from the present work. The Eisberg and Igo cross section is 80 millibarns greater than the (p,pxn) sum at 31 Mev, and this difference can be represented approximately as follows:

$$\sigma(p,p\gamma) + 2\sigma(p,2p) - \sigma(p,d) - \sigma(p,t) = 80 \text{ millibarns}$$

The (p,2p) cross section is probably at least as small as the (p,t)
cross section[24], and if the (p,d) cross section is taken to be
40 millibarns, a value of about 120 millibarns is obtained for
the (p,pγ) (or(p,pxn), x = o) cross section. This is roughly the
value that is obtained if a cross section curve like the (p,p2n)
one is shifted to a threshold 10 Mev lower than the (p,pn) threshold,
and reduced in magnitude by a typical barrier penetration factor
(see for example reference (7)). Finally, the Eisberg and Igo
cross section, and hence the (p,pxn) sum at 31 Mev from the present
work, are consistent in magnitude with the predictions of the diffuse
edge collision model[18].

A comparison of (p,pxn) cross sections from the present
work with (p,xn) cross sections for heavy elements measured by Bell
and Skarsgard[2] shows an interesting feature. The (p,p2n) cross
section at 50 Mev is about as large as the (p,3n) cross section at
the same bombarding energy. (This is above the energy where com-
pound nucleus processes contribute to the (p,3n) reaction.) The
(p,p2n) reaction probably arises when the incident proton is
scattered by a proton or a neutron in the diffuse nuclear edge, and
according to the mechanism that has been outlined above, the incident
proton, or a struck proton, escapes and residual excitation energy
results in the evaporation of 2 neutrons. This same mechanism as
well as the volume direct interaction mechanism[9] can lead to (p,3n)
reactions, and it might at first be expected that (p,3n) events would

predominate over (p,p2n) events; a closer examination, however,
shows that this expectation is not justified. Let us assume that
the ratio of neutron density to proton density is the same every-
where in the nucleus, including the diffuse edge. A (p,p2n)
reaction may occur when the incident proton strikes a proton, and
either of them escapes, or when the incident proton strikes a
neutron and the proton escapes. A (p,3n) reaction can only occur
when the struck particle is a neutron, and it alone escapes. Thus
in spite of the greater density of neutrons in the target, the
(p,p2n) cross section should be greater than the (p,3n) cross section,
so far as the diffuse edge mechanism is concerned. In other words,
a direct proton is more likely to come out because it was a proton
that went in. A crude estimate gives $\sigma(p,p2n)/\sigma(p,3n) = 2.3$. On
the other hand, Jackson's calculations show that at 50 Mev, the
interactions in the nuclear volume should give greater emphasis to
(p,3n) than to (p,p2n) reactions. The overall (p,p2n) and (p,3n)
cross sections thus should be roughly equal at 50 Mev, in agreement
with observation.

(b) Total Reaction Cross Section

Bell and Skarsgard[2] have measured the cross sections
for (p,xn) reactions in bismuth and lead, and the sum of the indivi-
dual (p,xn) cross sections for bismuth, as a function of incident
proton energy, is represented by the solid curve in Figure 18.

Fig. 18. The solid curve represents the sum
of (p,xn) cross sections for Bi^{209}, from reference
(2), and the circles result from the addition of
(p,pxn) cross sections from the present work to the
(p,xn) sum. The triangle at 31 Mev represents the
(p,xn) + (p,pxn) sum, plus a calculated (p,pγ) cross
section (see text). This latter cross section value
is a close approximation to the total reaction cross
section.

Figure 18   79a
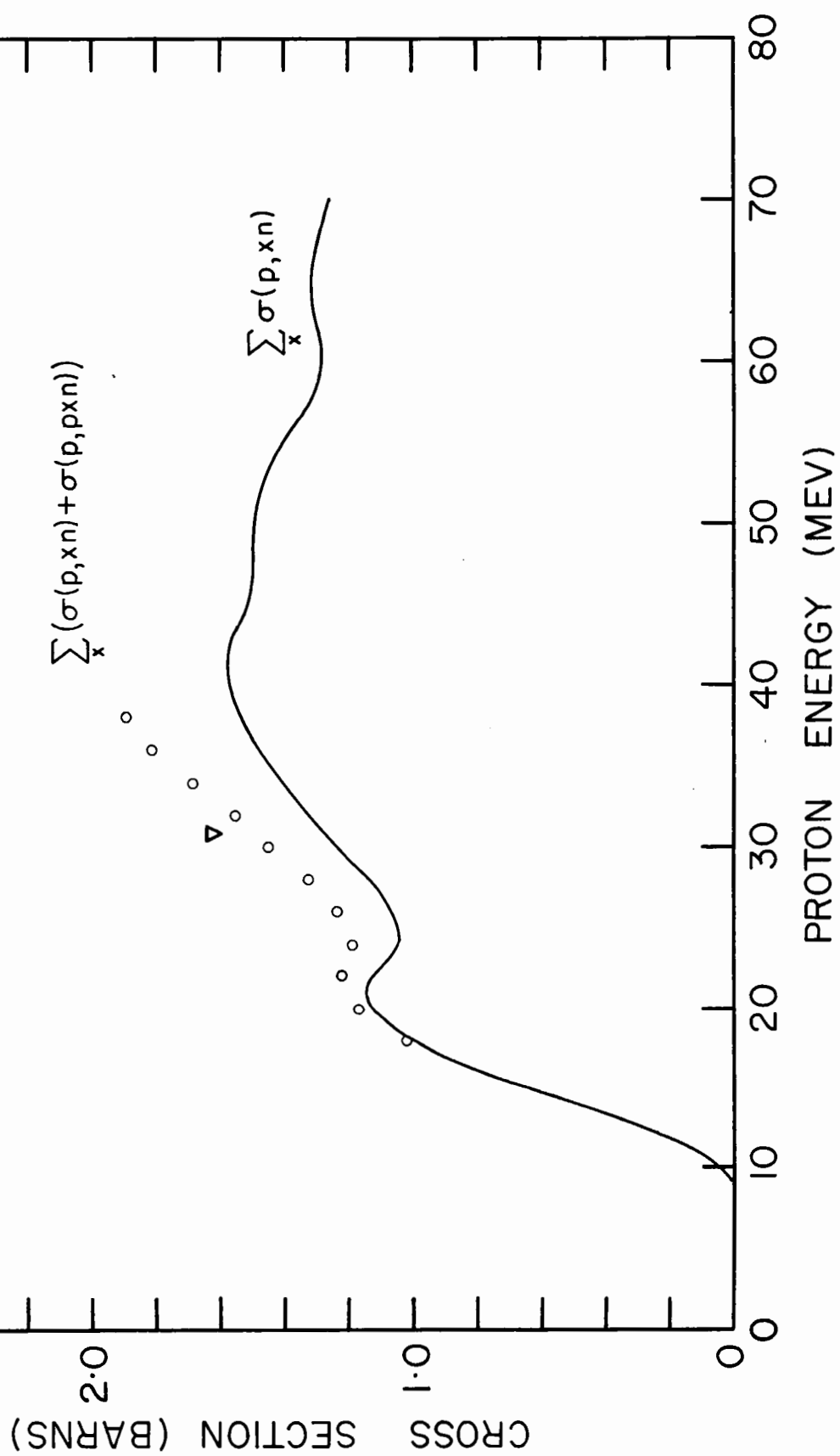
This curve has been adjusted here to be in accordance with a more recent carbon monitoring cross section[35]. The (p,xn) sum curve shows a pronounced minimum at about 25 Mev. The small circles show the present (p,pxn) results added to the (p,xn) sum. The triangle at 31 Mev represents the (p,xn) + (p,pxn) sum, plus the (p,pγ) cross section estimated in the previous section.

It is evident from Figure 18 that (p,pxn) reactions offer considerable competition to (p,xn) reactions for energies above the region of the hump in the (p,xn) curve. Since the (p,pxn) cross sections from the present work include (p,d) and (p,t) cross sections, and since (p,2pxn) cross sections are small [24][2], the triangular point in Figure 18 will be a good approximation to the total reaction cross section at 31 Mev. Furthermore, since the (p,pγ) cross section, which is important at 31 Mev, will rise from a threshold at about 10 Mev, it is reasonable to conclude that the total reaction cross section is a monotonic function of incident proton energy. This is in agreement with the predictions of the optical model[9]. Bell and Skarsgard were impelled toward an opposite conclusion because they did not know that the (p,pxn) cross sections were so large; however, the present work supports their observation that near the peak of any (p,xn) cross section, the (p,p(x-1)n) cross section is small by comparison.

It is pointed out that an addition of (p,pxn) cross sections for gold to (p,xn) cross sections for bismuth cannot be

rigorously accurate; however, reaction cross sections are not expected to vary strongly among heavy nuclei. The gold (p,pxn) cross sections were shifted x Mev toward lower energies in the addition, to account for the difference of about 1 Mev in the neutron binding energies for gold and bismuth. The geometrical cross section for gold will be slightly smaller than for bismuth, but the Coulomb barrier will also be lower. Bi^{209} and Au^{197} are both odd A, odd Z nuclei. Since the total (p,pxn) contribution to the sum curve is only about 20 percent, the addition procedure is correct to well within the errors in the experimental measurements. The sum of the (p,pxn) and (p,xn) cross sections is not shown in Figure 18 for incident proton energies greater than 40 Mev; above this energy (p,pxn) reactions for $x > 3$ become important, and these reactions have not been considered in the present work.

APPENDIX

THE ISOMERIC STATE IN AU^{196}

1. Introduction

Evidence for a 14 hour isomeric state in Au^{196} was reported by Wilkinson[43] in 1949. He made use of Geiger counters, and absorption experiments indicated that X-rays or soft gamma rays were emitted. It was concluded that decay of the isomeric state proceeds by electron capture or by an isomeric transition. Sosniak[29] reported a component with a half-life of about 14 hours in the K X-ray activity from Au^{196}.

In the study of (p,pn) cross sections in Au^{197} it is necessary to know something of the manner in which this isomeric state decays. At bombarding energies above the centrifugal barrier there will be a high probability of (p,pn) reactions leading to the isomeric state, and there is risk of error if cross section measurements are based only on ground state activity. The discussion which follows describes a study of the decay of the Au^{196} isomeric state. An investigation of this decay was carried out concurrently by Van Lieshout et al, and their results have recently been published[44]. For the most part, the results of the two investigations are in excellent agreement. Transition energy determinations in the present work, based on conversion

electron measurements using a high resolution magnetic spectro-
graph, are more precise than those of Van Lieshout et al; however
better low resolution measurements by the latter workers remove
ambiguities from multipolarity assignments based, in the present
work, on L-subshell conversion ratios.

2. Gamma Ray Measurements

Gold samples were bombarded at about 28 Mev and mercury
was removed by the slow distillation procedure described earlier
(Section III.3). Early experiments, using a sodium iodide scin-
tillation spectrometer, showed strong short-lived gamma rays at
about 150 and 190 kev, located on the Compton continuum from the
354 and 331 kev Au^{196} ground state gamma rays.

In order to separate these short-lived gamma rays from
the Compton background, two samples were bombarded at the same
proton energy, one week apart. The bombardment time for the second
sample was half that for the first, so that both samples had about
the same 6.1 day Au^{196} activity at the time of the second bombard-
ment. By this time the short-lived activity had disappeared from
the first sample. The "new" sample was counted using a 1 1/2 inch
diameter by 1 inch high NaI(Tl) crystal and the 256-channel kick-
sorter. The "old" source activity was then subtracted from the
spectrum, using the automatic background subtraction facility in

the kicksorter. Subtraction was continued until the total energy
peak due to the 354 and 331 kev gamma rays was reduced to zero.
The "adding" and "subtracting" times were approximately equal,
and source strengths were high enough so that room background
counts were effectively cancelled. This subtracting procedure
removed all effects due to the 6.1 day activity, leaving only
the spectrum of the shorter-lived activity; the resulting spectrum
is shown in Figure 19.

The energy scale for the gamma ray spectrum was deter-
mined from the 245 kev photopeak of Ce^{141}, the 279 kev peak from
Hg^{203}, and K X-ray peaks from Au^{196} and Hg^{203} sources. These
calibration points are represented by arrows along the top of
Figure 19. This calibration gave energies of 148 ± 2 kev and
188 ± 2 kev for the gamma rays resulting from the decay of Au^{196m}.
The arrows along the bottom of Figure 19 represent transition
energies determined from 180° spectrograph measurements of con-
version electrons. The broad peak centred in channel 100 is
probably due to small amounts of Au^{194} produced in (p,p3n) reac-
tions.

Figure 20 shows the gamma ray spectrum recorded by a 5
inch diameter by 5 inch high NaI(Tl) scintillation crystal used in
conjunction with a single-channel analyzer. The large crystal
strongly reduces Compton background from the high energy gamma rays.
The 148 and 188 kev peaks are seen, though they are not as well

Fig. 19. Pulse height spectrum from Au^{196m} radiation detected by a sodium iodide scintillation counter (crystal size 1 1/2 inches by 1 inch). The arrows along the top of the graph represent energy calibration points, and the arrows along the bottom designate transition energies determined from conversion electron measurements. The spectrum due to the 6.1 day Au^{196} ground state has been subtracted by a technique described in the text. The broad peak centered in channel 100 is due to Au^{194} activity.

Figure 19

85a

Figure 19
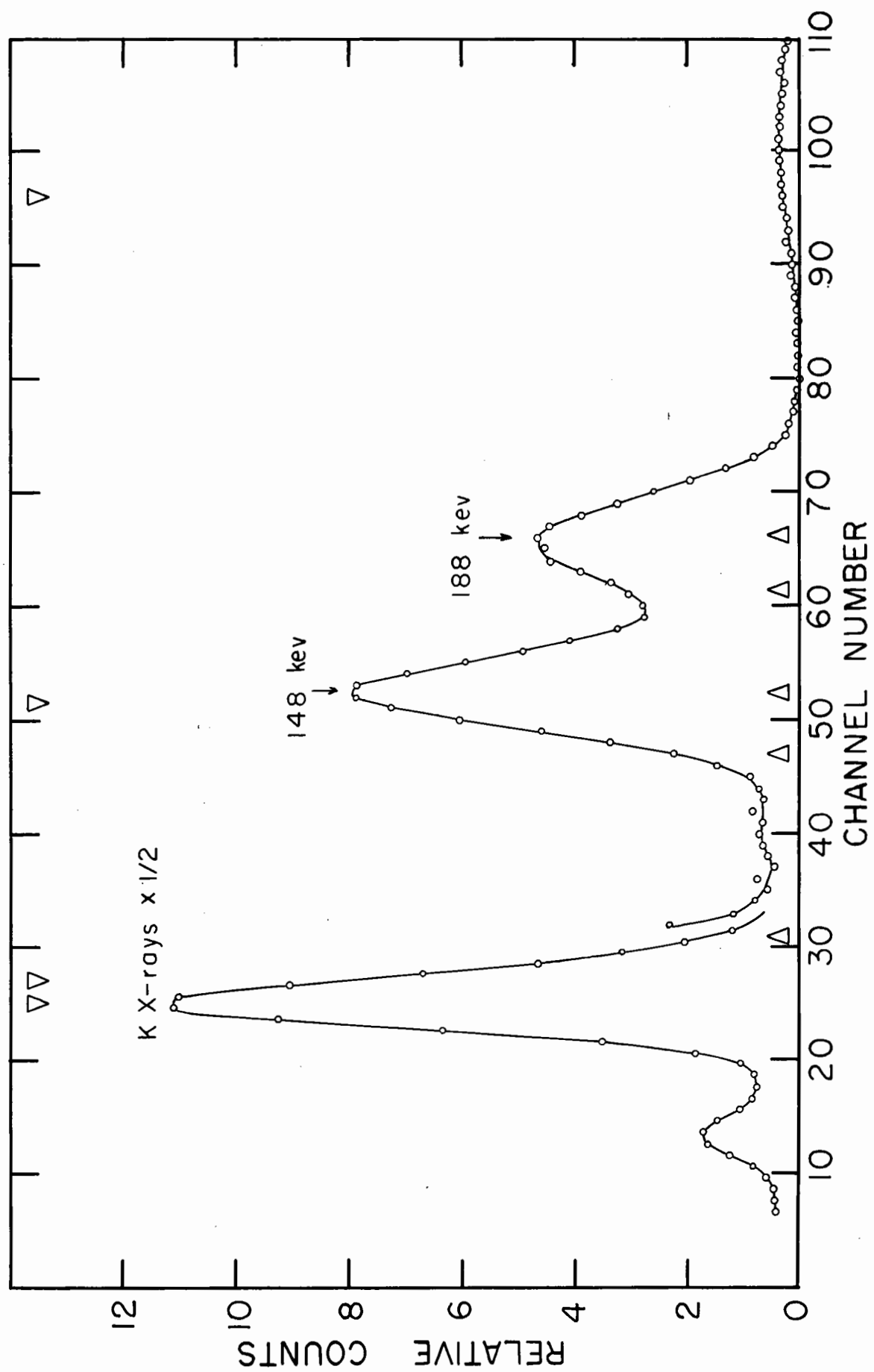
Fig. 20. Pulse height spectrum from Au^{196} and Au^{196m} radiation detected by a sodium iodide counter (crystal size 5 inches by 5 inches). The open circles represent the spectrum soon after preparation of the source, and the closed circles show the spectrum from the same source after about 6 days. The dashed vertical lines enclose a portion of the spectrum used to determine the half-life of Au^{196m}(see text and Fig. 21).

Figure 20

K X-rays

148 kev

188 kev

354 kev
and
332 kev

RELATIVE COUNTING RATE

PULSE HEIGHT

86a

resolved as in Figure 19. The lower curve shows the spectrum after about 6 days.

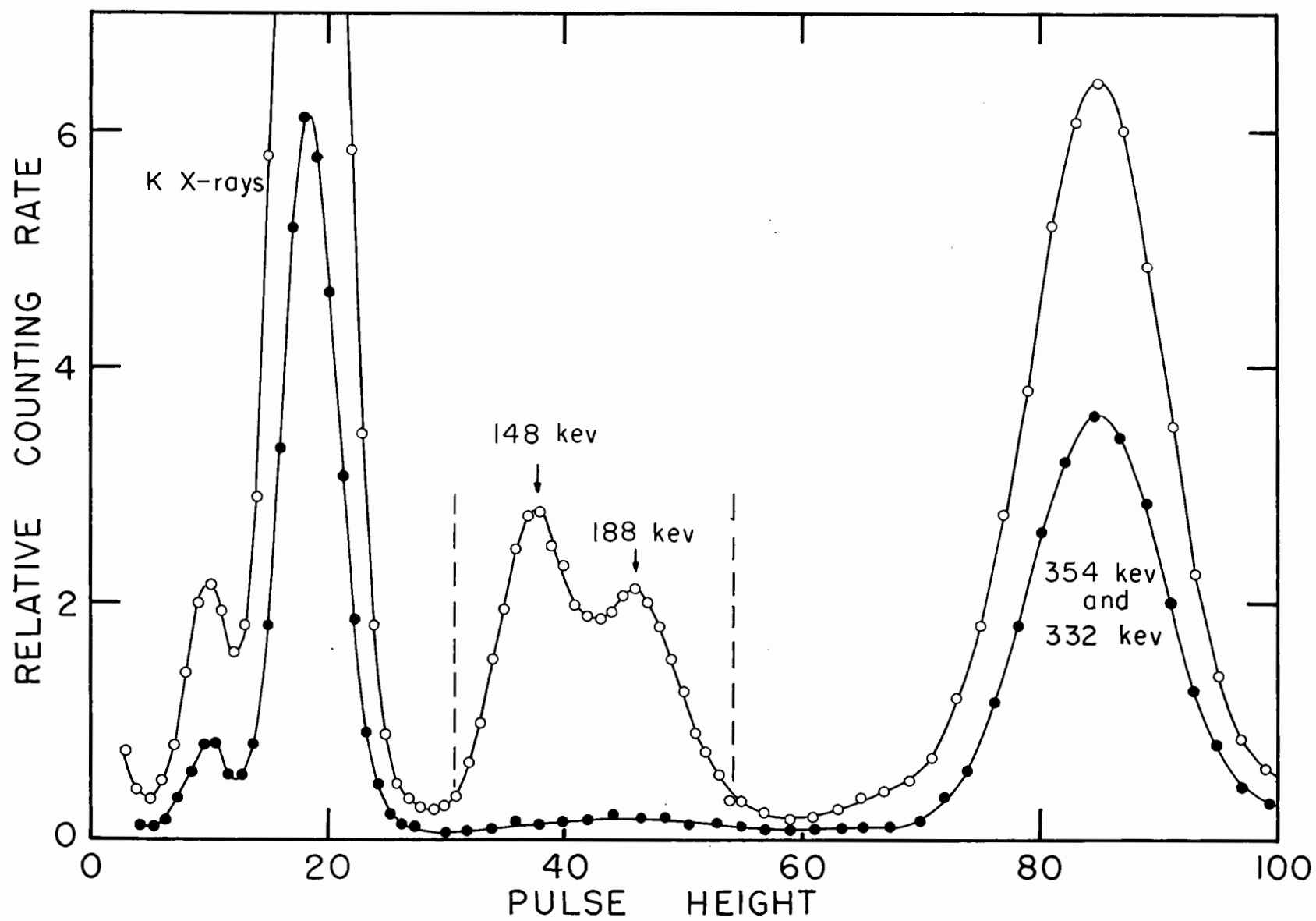Measurements were carried out using the high efficiency sodium iodide scintillation counter described earlier (two 1 1/2 inch by 1 inch sodium iodide counters placed in contact, with the source sandwiched between them). Subtraction techniques, using "new" and "old" sources indicated a strong sum peak at about 335 kev, and it is concluded that the 148 and 188 kev gamma rays are emitted in coincidence.

3. Half-Life Determination

A gold foil was bombarded with 28 Mev protons, and after separation of mercury, the gamma ray spectrum was recorded with a 5 inch by 5 inch sodium iodide crystal and single-channel analyzer arrangement. The spectrum is represented by the open circles in Figure 20. The single-channel analyzer window was then set to pass pulses in the 148 and 188 kev total energy peaks. The window boundaries are represented by the dashed vertical lines in Figure 20. The output pulses from the analyzer were fed to a counting-rate meter and Esterline-Angus chart recorder combination that automatically recorded the decay of the isomeric state activity. Since the large crystal gave a low Compton continuum from the ground state gamma rays, the magnitude of the 6.1 day component in the decay curve is much smaller than would be the case if a

88

small crystal were used; the determination of the half-life of the short-lived activity is thus more precise. The resulting decay curve is shown in Figure 21. A second spectrum was recorded after about six days, and it is represented by the closed circles in Figure 20.

The composite decay curve shown in Figure 21 gives a value of 9.5 ± 0.3 hours for the half-life of the short-lived activity. This in disagreement with the value of 14.0 ± 0.3 hours reported by Wilkinson, but in agreement with the value of 10.0 ± 0.5 hours given by Van Lieshout et al.

4. Conversion Electron Measurements

Measurements of the conversion electron spectrum of Au^{196} and Au^{196m} were made with both a high resolution 180° magnetic spectrograph[50] and a Slätis-Siegbahn type magnetic spectrometer[51][52].

It is difficult to prepare conversion electron sources of Au^{196m} by proton bombardment. Since (p,pn) reactions lead to isotopes of the target element, carrier free sources cannot be prepared in this way. Only a very small amount of target material can be used if a thin spectrometer source is desired, and consequently the activity produced is low. Carrier free gold sources could be prepared from products of (p,xn) reactions in platinum, but even with enriched isotopes the complex spectrum from 17.5

Fig. 21. Decay curve of Au^{196m} and Au^{196}
activity. The upper curve represents the experi-
mental measurements, and subtraction of the 6.1
day Au^{196} component from the gross decay curve in-
dicates that the isomeric state has a half-life of
9.5 ± 0.3 hours.

Figure 21
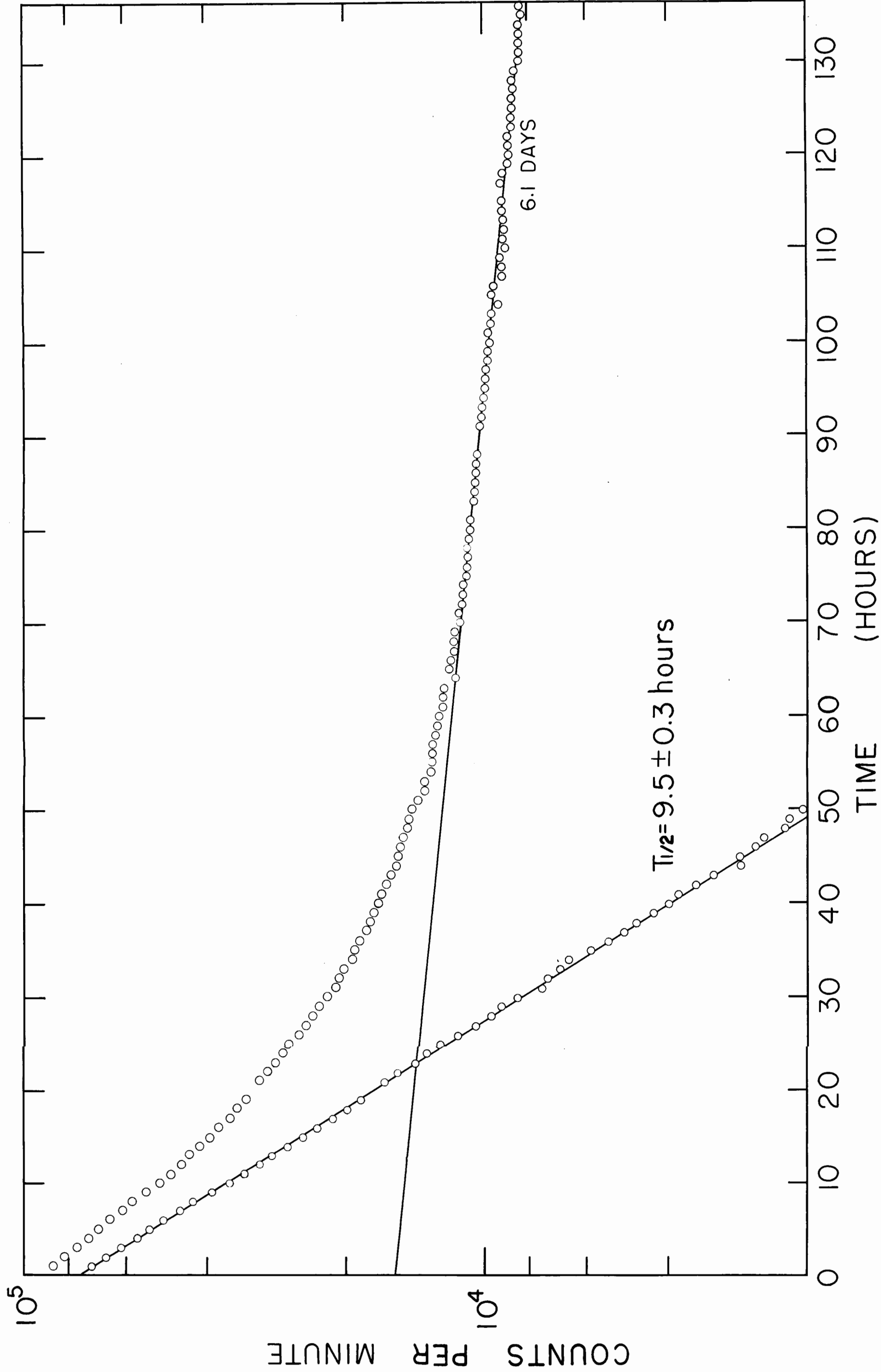
hour Au^{193} would probably interfere prohibitively with measure-
ments of Au^{196m}. Sources used in the present experiments were
obtained from (p,pn) reactions.

(a) 180° Spectrograph Measurements

A strip of gold foil 0.001 inches thick by 0.01 inches
wide, and about 0.75 inches long was folded double and mounted
radially on the cyclotron probe in such a manner that the beam
was normal to the 0.010 inch dimension. Preliminary experiments
showed that this arrangement would probably give optimum specific
activity for a source of the required dimensions. The folding
doubled the thickness of the target "seen" by the beam, and the
radial penetration for a target of 0.010 inches vertical dimension
concentrates a majority of the activity fairly uniformly along the
first 1/4 inch from the tip. The unfolded source was thus about
1/2 inch long, suitable for the spectrograph. The sample was bom-
barded for 8 hours, and after removal of mercury was mounted directly
in the spectrograph.

The photographic plate in the spectrograph was exposed
for 3 days. A masking procedure was used to give an indication of
the half-lives of the conversion lines. A strip 1/3 the width of
the plate and along one edge of the plate was masked for a period
of 9.5 hours, and then the mask was reversed to cover the opposite
edge of the plate for the remainder of the exposure. The centre

1/3 of the plate was thus exposed for the whole period, and lines with a half-life of 9.5 hours appear with equal blackening on the two outer portions of the plate. The plate showed 29 conversion lines. Due to the width and thickness of the source, the lines were fairly broad, but the resolution was sufficient to clearly resolve L_I, L_{II} and L_{III} components. The magnetic field of the spectrograph was calibrated using a radio-thorium source.

The positions of the lines on the plate were measured with a comparator, and the results are shown in Table III. Comparator readings were taken from the high energy edge of the broad lines. Electron energies are estimated to be accurate to within ± 0.2 kev, and to establish a transition, the various electron energies together with the binding energy in the assigned shell were required to add to within 0.4 kev. The transition energies are considered to have a standard error of about 0.5 kev.

The decay of the isomeric state involves isomeric transitions of energies 148.2 ± 0.5 kev, 175.5 ± 0.5 kev and 188.8 ± 0.5 kev. A weak 135.9 ± 0.5 kev transition converted in Pt indicates a small electron capture branch. Table III also shows an 85.0 kev transition, but the absence of the K-line prevents definite establishment of the origin of the transition; however, relative intensities of the 85.0 and 175.5 kev lines indicate that they are probably in cascade. The energy assignment of 85.0 kev assumes conversion in Au, but the energies add nearly as well to

TABLE III

180° Spectrograph Data

Line	Conversion Electron Energy	Probable Half-Life	Assignment
1	51.1 kev		Auger
2	52.8		"
3	53.3		"
4	55.2		"
5	57.4 (weak)	9.5 hours	K 135.9 kev transition in Pt
6	61.7		Auger
7	63.9		"
8	67.3	9.5 hours	K 148.2 kev transition in Au
9	71.3	"	L_{II} 85.0 kev transition
10	73.1	"	L_{III} 85.0 kev "
11	81.9	"	M_{II} 85.0 kev "
12	87.8	<9.5 hours	?
13	94.6	9.5 hours	K 175.5 kev " in Au
14	108.1	"	K 188.8 kev " "
15	122.1 (weak)	"	L_I 135.9 kev " in Pt
16	124.3 (weak)	"	L_{III} 135.9 kev " "
17	134.6	"	L_{II} 148.2 kev " in Au
18	136.4	"	L_{III} 148.2 kev " "
19	143.7 (weak)	"	M 148.2 kev " "
20	145.4 (weak)	"	M 148.2 kev " "
21	161.1	"	L_I 175.5 kev " "
22	163.8	"	L_{III} 175.5 kev " "
23	172.3	"	M_I 175.5 kev " "
24	172.9	"	M_{III} 175.5 kev " "
25	174.9	"	L_I or L_{II} 188.8 kev "
26	255.6	6.1 days	K 334.0 kev " in Pt
27	275.7 (weak)	"	K 354.1 kev " " ?
28	278.4	"	K 356.8 kev " "
29	343.1	"	K 426.3 kev " in Hg or
			L_I 356.8 kev " in Pt

fit an 84.7 kev transition in Pt. It should also be pointed out that lines 14, 23, 24 and 25 are consistent with the assignment K, L_I, L_{II}, L_{III} respectively for a 186.3 kev transition in Pt. However, the assignments as indicated in the table are probably correct, since gamma ray measurements (in this work and in reference (44)) indicate that this transition is in coincidence with the 148.2 kev gamma ray. The conversion lines for the 175.5 kev and 85.0 kev transitions are relatively very intense, and the 135.9 kev lines very weak. The transition energies determined from these experiments are indicated by the arrows along the bottom of Figure 19.

Relative intensities of the L-lines indicate that the 175.5 kev transition is probably M4, and the other multipolarity assignments are less certain. The 148.2 kev transition is likely E2, but relative intensities are consistent with the assignment of a higher electric multipolarity. The 85.0 kev transition can be electric with multipolarity 2 or greater, the 135.9 kev transition can be M3 or M4, and the 188.8 kev transition E1, M1 or M2. Most of these ambiguities are removed by the work of Van Lieshout et al.

Conversion lines from decay of the 6.1 day ground state of Au^{196} are also shown in Table III, and the results agree fairly well with those of previous investigations[45]. Most previous workers report lines due to 332 kev and 354 kev transitions in

Pt^{196}, and a 426 kev transition in Hg^{196}, but Kane and Frankel[53] report energies of 334.0 kev and 356.5 kev for the transitions in Pt^{196}, in excellent agreement with the present work. There is, however, a very weak line that could be interpreted as the K-line for a 354.1 kev transition.

(b) Slätis-Siegbahn Spectrometer Measurements

Sources for this instrument were prepared by vacuum evaporation. The crucible used was made by pressing a conical indentation into a piece of 0.001 inch thick tungsten ribbon. A 0.0001 inch thick copper foil was placed about 1/16 of an inch above the crucible and the evaporated gold was deposited on this foil in a 1/8 inch diameter spot, suitable for a spectrometer source. The evaporation was done rapidly, and typical yields after two "flashings" were about 30 percent. Further flashing formed spots that were too large, due to the tendency of the gold to creep out of the crucible.

Strips of 0.001 inch thick gold foil about 0.01 inches wide were mounted radially on the cyclotron probe, and were bombarded for from 2 to 3 hours. A 2 mm long portion was cut from the target tip after bombardment, and evaporated onto a copper foil as described above. This procedure gave sources of high specific activity, and when the small mass of gold was deposited

on a 1/8 inch spot the source thickness was of the order of 10^{-5} inches. Due to the vertical oscillation of the cyclotron beam, this method produces higher specific activity than would be obtained by bombarding a target 10^{-5} inches thick.

A typical spectrometer record is shown in Figure 22. The magnetic field of the spectrometer was calibrated from conversion lines due to the 6.1 day Au^{196} ground state activity (these lines are not shown on the figure). Since the sources were very weak it was difficult to distinguish lower energy conversion lines from the detector tube noise, and it was necessary to use a discriminator bias which also discriminated against the lower energy lines shown on the graph. In this graph no correction has been made for discrimination losses. The corrected results are somewhat unreliable, but give K/L conversion ratios consistent with those given by Van Lieshout et al.

Decay curves were obtained for the 5 most prominent lines and they indicated similar half-lives of 11 ± 2 hours.

5. Discussion

The results of the experiments that have been described are in excellent agreement with the work of Van Lieshout et al, and the decay scheme proposed by these authors is confirmed. The transition energies as determined in the present measurements are more precise than those given by Van Lieshout et al, and in some

Fig. 22. Conversion electron spectrum of Au^{196m}
obtained with a Slätis-Siegbahn type magnetic spectro-
meter. The spectrum is distorted due to discrimination
by the detector against low energy electrons. Conver-
sion electron peaks are labelled with transition energies
and a designation of the electron shell in which the
transition was converted. The transition energies shown
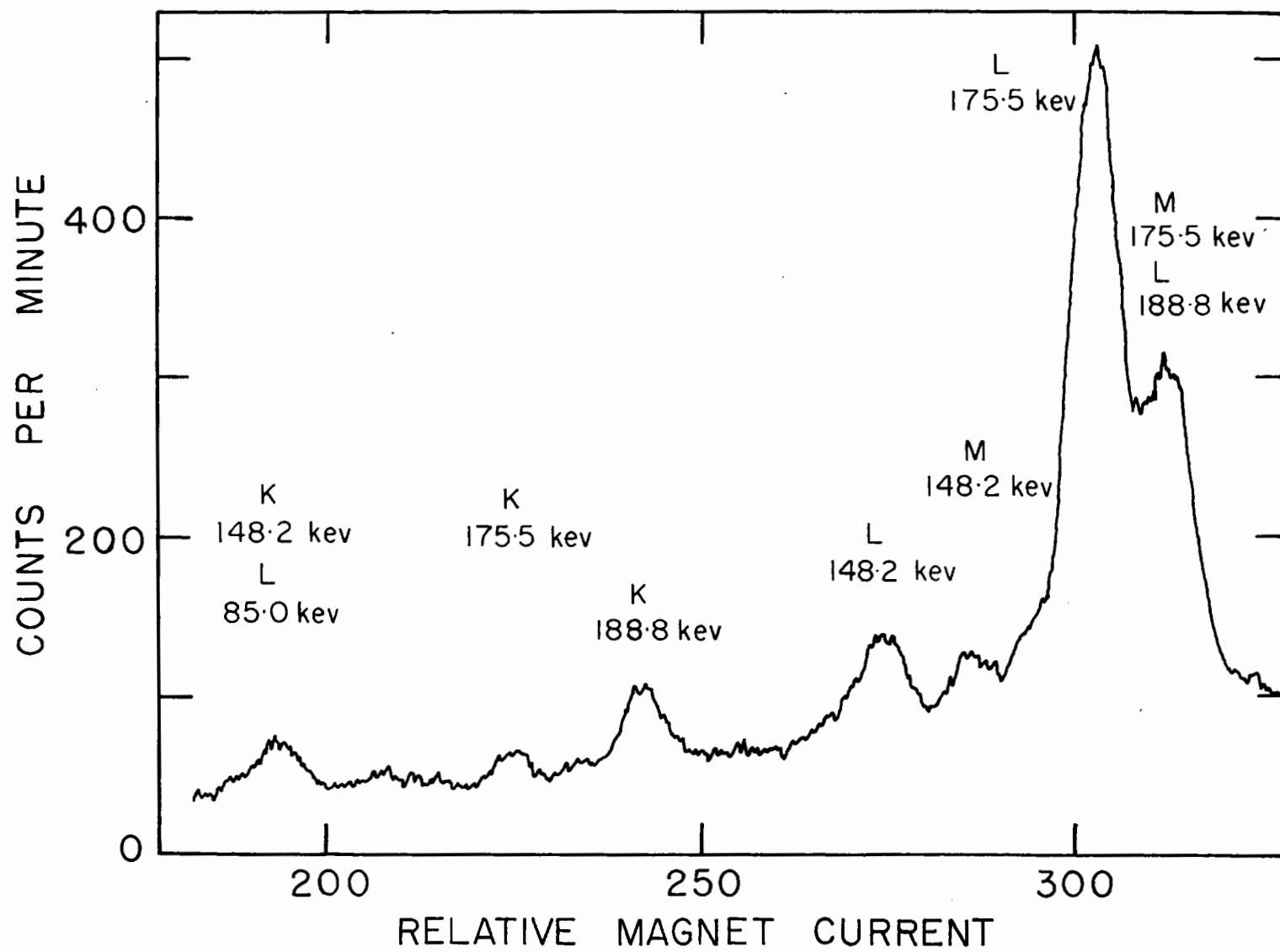are from high resolution 180° spectrograph measurements
(see text).

Figure 22

cases L-subshell conversion ratios from the 180° spectrograph results reported here remove ambiguity in the multipolarity assignments made by these workers.

The isomeric state decays initially by an M4 transition with an energy of 175.5 ± 0.5 kev. The Weisskopf estimates[54] for such a transition are consistent with the measured half-life of 9.5 ± 0.3 hours. There are two transitions in gold of energies 188.8 ± 0.5 and 148.2 ± 0.5 kev which are in cascade, and coincidence experiments by Van Lieshout show that these are also in cascade with the 175.5 kev transition. The multipolarities of the 188.8 and 148.2 kev transitions are well established by the L-subshell conversion ratios from the present work and the K/L conversion ratios from the measurements of Van Lieshout et al. The 148.2 kev kev transition is probably pure E2, and the 188.8 kev transition is likely an M1. The absence of the 188.8 kev L_{III} line in the present results indicates that the E2 admixture considered by Van Lieshout for the 188.8 kev transition must be small. An 85.0 ± 0.5 kev transition, tentatively proposed by Van Lieshout et al has been definitely established by the high resolution conversion electron measurements described here. This transition probably has multi-polarity E2. The absence of the K conversion line for the 85.0 kev transition makes it impossible to establish that it is con-verted in gold, but relative intensities of conversion lines in-dicate that this transition may be in cascade with the 175.5,

188.8 and 148.2 kev transitions. The order of the transitions following the initial 175.5 kev one has not been established.

A transition of 135.9 ± 0.5 kev, converted in platinum, has been observed in the present experiments and this indicates a small electron capture branch. Since the conversion lines associated with this transition are very weak, and since no unconverted gamma rays of this energy are observed, it is concluded that the electron capture branching ratio is small, and probably less than 10 percent. Van Lieshout et al report no evidence for this transition; however, in the present work the weak conversion lines were seen only in the high resolution 180° spectrograph experiment. The Van Lieshout experiments do however support the conclusion that the electron capture probability is small.

The decay scheme of the Au^{196} isomeric state, as indicated by the experiments that have been described, is shown in Figure 23. Except for the small electron capture branch, this decay scheme is similar to that given by Van Lieshout et al.

A theoretical interpretation of the decay scheme is difficult. The isomeric state spin is very high, probably 11+, and an h 11/2 proton shell and a g 9/2 neutron shell are likely involved. However, for this odd-odd nucleus the uncertain coupling of the odd neutron and odd proton spins makes an interpretation very ambiguous.

Fig. 23. Decay scheme of Au^{196m}. The order of the 3 lower transitions in gold is not known. Except for the small electron capture branch, this decay scheme is similar to that proposed in reference (44). The transition which follows electron capture is probably in cascade with the 332 and 354 kev transitions which follow electron capture in the ground state (see Fig. 6).

Figure 23   99a
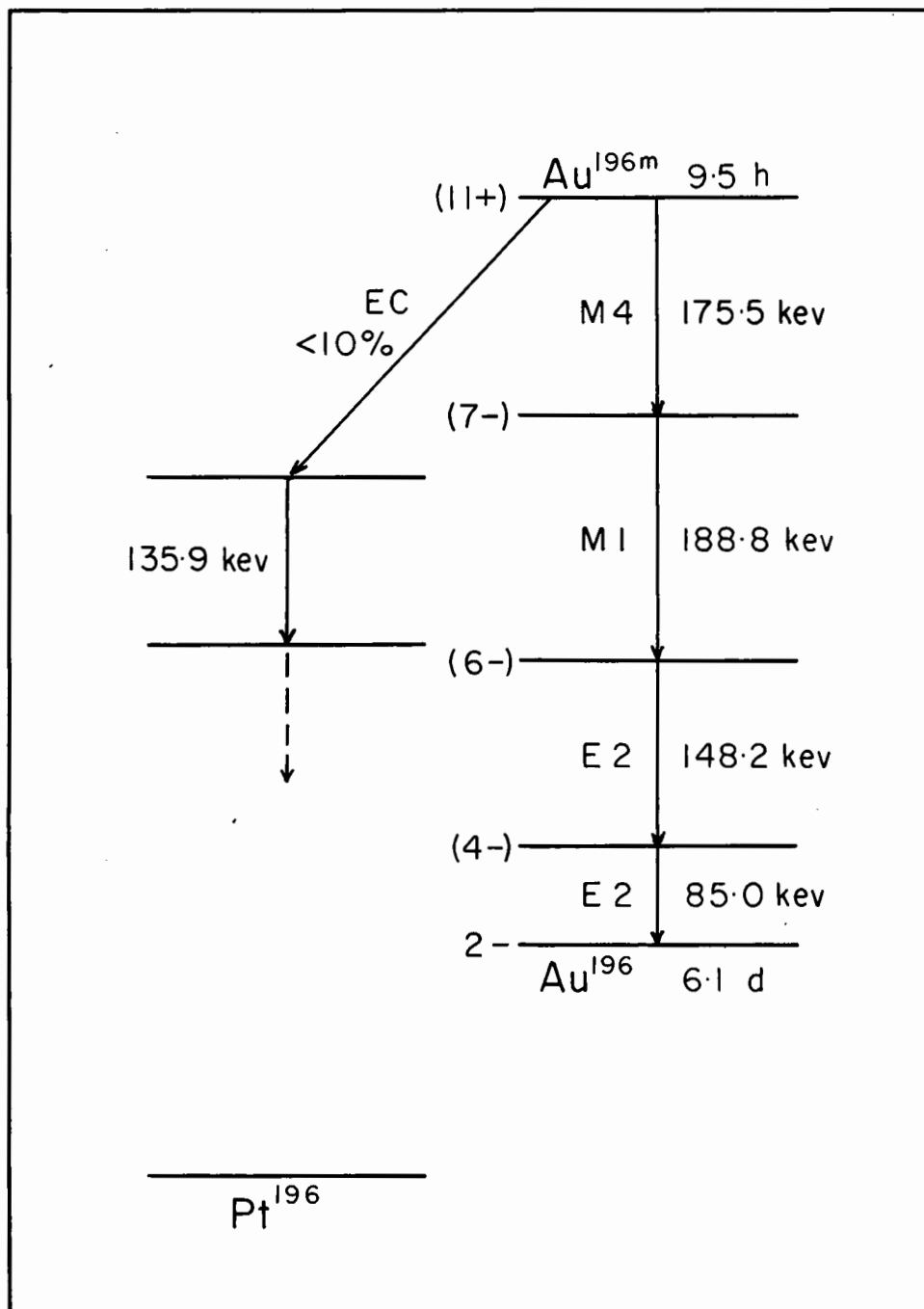
BIBLIOGRAPHY

(1) R.M. Eisberg and E. Igo, Phys. Rev. $\underline{93}$, 1039 (1954).

(2) R.E. Bell and H.M. Skarsgard, Can. J. Phys. $\underline{34}$, 745 (1956).

(3) T.M. Kavanagh and R.E. Bell, Annual Congress of the Canadian Association of Physicists, June 1959.

(4) S.A. Moszkowski, Handbuch der Physic Vol. 39, (1957).

(5) P.M. Endt and M. Demeur, "Nuclear Reactions", North-Holland Pub. Co., Amsterdam, 1959.

(6) J.M. Blatt and V.F. Weisskopf, "Theoretical Nuclear Physics", John Wiley and Sons Inc., New York, 1952, p. 352-353.

(7) M. Shapiro, Phys. Rev. $\underline{90}$, 171 (1953).

(8) R. Serber, Phys. Rev. $\underline{72}$, 1114 (1947).

(9) J.D. Jackson, Can. J. Phys. $\underline{34}$, 767 (1956).

(10) H. Feshbach, C. Porter and V.F. Weisskopf, Phys. Rev. $\underline{96}$, 448 (1954).

(11) R. Hofstadter, Revs. Mod. Phys. $\underline{28}$, 214 (1956).

(12) W.J. Swiatecki, Proceedings of the University of Pittsburgh Conference on Nuclear Structure (1957).

(13) B.L. Cohen, Phys. Rev. $\underline{105}$, 1549 (1957).

(14) B.L. Cohen and S.W. Mosko, Phys. Rev. $\underline{106}$, 995 (1957).

(15) B.L. Cohen and A.G. Rubin, Phys. Rev. $\underline{114}$, 1143 (1959).

(16) N. Austern, S.T. Butler and H. McManus, Phys. Rev. $\underline{92}$, 350 (1953).

(17) C.A. Levinson and M.K. Banerjee, Annals of Phys. $\underline{2}$, 471 (1957).

(18) L.R.B. Elton and L.C. Gomes, Phys. Rev. $\underline{105}$, 1027 (1957).

(19) S. Hayakawa, M. Kawai and K. Kikuchi, Prog. Theor. Phys. $\underline{13}$, 415 (1955).

(39) M.E. Rose, "Internal Conversion Coefficients", North-Holland
Pub. Co., Amsterdam, 1958.

(40) C.M. Davisson, "Beta- and Gamma-Ray Spectroscopy", edited by
K. Siegbahn, North-Holland Pub. Co., Amsterdam, 1955, p. 857.

(41) M.T. Thieme and E. Bleuler, Phys. Rev. 101, 1031 (1956).

(42) P. Stähelin, Phys. Rev. 87, 374 (1952).

(43) G. Wilkinson, Phys. Rev. 75, 1019 (1949).

(44) R. Van Lieshout, R.K. Girgis, R.A. Rici and A.H. Wapstra,
Physica 25, 703 (1959).

(45) D. Strominger, J.M. Hollander and G.T. Seaborg, Revs. Mod.
Phys. 30, 585 (1958).

(46) A. Bisi, E. Germagnoli and L. Zappa, Nuovo Cimento 11, 843
(1959).

(47) A. de Shalit, O. Huber and H. Schneider, Helv. Phys. Acta 25,
279 (1952).

(48) M.T. Thieme and E. Bleuler, Phys. Rev. 102, 195 (1956).

(49) P.F. Zweifel, Phys. Rev. 96, 1572 (1954). ibid. 107, 329 (1957).

(50) F.A. Johnson, PhD Thesis, McGill University, 1952.

(51) E.R. Epp, PhD Thesis, McGill University, 1955.

(52) J.W. Hilborn, PhD Thesis, McGill University, 1955.

(53) J.V. Kane and S. Frankel, Bull. Am. Phys. Soc. Ser. 11, 2, 25
(1957).

(54) S.A. Moszkowski, "Beta- and Gamma-Ray Spectroscopy", edited by
K. Siegbahn, North-Holland Pub. Co., Amsterdam, 1955, p. 392.